Bioorganic Chemistry 121 (2022) 105664

Contents lists available at ScienceDirect

Bioorganic Chemistry

journal homepage: www.elsevier.com/locate/bioorg

Indirubin-3′-alkoxime derivatives for upregulation of Wnt signaling through dual inhibition of GSK-3β and the CXXC5-Dvl interaction

Doona Song [a,c], Yunja Lee [d], Min-Jeong Kang [d], Jae Won Kim [a], Soung-Hoon Lee [a], Kang-Yell Choi [a,d], Eun-Yeong Kim [e], Kiho Lee [e], Gyoonhee Han [a,b,*]

[a] Department of Biotechnology, College of Life Science and Biotechnology, Yonsei University, Seoul 03722, Korea
[b] Department of Pharmacy, College of Pharmacy, Yonsei University, Incheon 21983, Republic of Korea
[c] Graduate Program of Industrial Pharmaceutical Science, College of Pharmacy, Yonsei University, Yeonsugu, Incheon 21983, Republic of Korea
[d] CK Regeon Inc., Seoul 03722, Republic of Korea
[e] College of Pharmacy, Korea University, Sejong 339-700, Republic of Korea

ARTICLE INFO

Keywords:
Indirubin-3′-alkoxime derivatives
Wnt signaling
GSK-3β
CXXC5-Dvl interaction
Dual inhibition
Wound healing

ABSTRACT

Glycogen synthase kinase-3β (GSK-3β) appears to be ordinarily expressed, and functionally redundant in Wnt/β-catenin signaling. The Wnt proteins induce transduction of a cytoplasmic protein, Dishevelled (Dvl) which negatively modulates GSK-3β activity. CXXC5 is a negative modulator of the Wnt/β-catenin signaling through the interaction with Dvl in the cytosol. This indicates that Wnt/β-catenin signaling could be efficiently modulated by controlling GSK-3β and the CXXC5-Dvl interaction. In this study, we designed a series of indirubin-3′-oxime and indirubin-3′-alkoxime derivatives containing various functional groups at the 5- or 6-position (R_1) alongside alkyl or benzylic moieties at the 3′-oxime position (R_2). These activate Wnt signaling through inhibitions of both GSK-3β and the CXXC5-Dvl protein–protein interaction, in addition, the improvement of pharmacological properties. The potent activity profiles of the synthesized compounds suggested that dual inhibition of GSK-3β and the CXXC5-Dvl interaction could be an appropriate approach towards safely and efficiently activating Wnt signaling. Thus, dual-targeting inhibitors are potentially better candidates for efficient activation of Wnt -signaling compared to GSK-3β inhibitors.

1. Introduction

Glycogen synthase kinase-3β (GSK-3β) ubiquitously acts as a multifunctional protein kinase through phosphorylation of Ser/Thr residues of substrates [1]. GSK-3β regulates various functions in the cell, including cell proliferation, cell survival, gene expression, cellular architecture, neural development and plasticity etc. [2]. GSK-3β appears to be ordinarily expressed, and functionally redundant in some signaling pathways, including Wnt/β-catenin signalling [3]. There are two Wnt signaling pathways: the β-catenin dependent pathway is referred to as the canonical Wnt signaling pathway, whereas the β-catenin independent pathway is the noncanonical Wnt signaling pathway [4]. In canonical Wnt signaling, GSK-3β-mediated phosphorylation leads to destabilized β-catenin which is identified as a GSK-3β substrate [5]. In the absence of the Wnt signal, GSK-3β leads to stabilization of the multiprotein complex and phosphorylates β-catenin, which is a multifunctional protein originally identified as a cadherin-associated protein [6]. Thus, GSK-3β in the destruction complex promotes β-catenin degradation [7]. Conversely, stabilization of β-catenin by the Wnt signal results in its association with the high mobility group (HMG)-domain proteins, the Lef/Tcf family transcription factors, which then alters the expression of target genes [8]. The Wnt proteins interact with Frizzled, a family of G proteins-coupled receptors, and induce transduction of a cytoplasmic protein, Dishevelled (Dvl). Dvl, activated by the Wnt signal, negatively modulates GSK-3β activity [9]. CXXC5 is a negative modulator of the Wnt/β-catenin signaling through an interaction with Dvl in the cytosol [10]. Blockade of the CXXC5–Dvl interaction affects various pathophysiological phenotypes, including wound healing, osteoporosis, and hair loss through the activation of Wnt/β-catenin signalling [11]. In the case of wound healing, activation of Wnt/β-catenin signaling by wound formation, serves as a positive stimulus for wound repair, through activation of stem cells and induction of their self-renewal and proliferation [12]. Moreover, β-catenin is also increased during the proliferative phase of wound repair [13]. Furthermore, the Wnt signals are

* Corresponding author at: Department of Biotechnology, Yonsei University, Seoul 03722, Republic of Korea..
E-mail address: gyoonhee@yonsei.ac.kr (G. Han).

https://doi.org/10.1016/j.bioorg.2022.105664
Received 4 November 2021; Received in revised form 27 January 2022; Accepted 5 February 2022
Available online 8 February 2022

necessary for recovering epithelial tissue patterning during wound healing [14]. The use of GSK-3β inhibitors, such as valproic acid, effectively promotes wound healing in small cutaneous wounds through the Wnt signaling pathway [14,15]. However, valproic acid does not effectively accelerate cutaneous wound healing in large or chronic wounds, because the negative Wnt regulator, CXXC5 is increased [16]. Alternatively, combination treatment with valproic acid and peptides that inhibit the CXXC5-Dvl interaction significantly promote cutaneous wound healing in large wounds [16]. Thus, the dual inhibition of the CXXC5-Dvl interaction and GSK-3β could be efficient in activating the Wnt/β-catenin signaling.

The bis-indole indirubin (Fig. 1) is known as the active ingredient of the traditional Chinese medicine recipe Danggui Longhui Wan, which is used against chronic myelocytic leukemia. However, indirubin is not acknowledged as a drug because of its poor solubility, low absorption and gastrointestinal toxicity [17]. Several indirubin analogs, such as *N*-methylisoindigo and indirubin-3′-oxime (Fig. 1), have therefore been synthesized to provide improved pharmacological properties and reduced toxicity [18,19]. Indirubin and their synthetic analogs such as 6-bromoindirubin-3′-oxime (BIO, Fig. 1) were reported as selective inhibitors of GSK-3β [20]. Here, an indole ring that was included in the structure on BIO and I3O could interact with the PDZ domain [21]. Similarly, BIO and I3O also affected the CXXC5-Dvl interaction [22]. Thus, indirubin analogs could inhibit both GSK-3β and the CXXC5-Dvl protein–protein interaction.

In this study, we designed a series of indirubin-3′-oxime and indirubin-3′-alkoxime derivatives by introducing various functional groups at either the 5- or 6-position (R_1 group). In addition, alkyl or benzylic moieties were also added at the 3′-oxime position (R_2 group) to inhibit the activity of both GSK-3β and the CXXC5-Dvl interaction, alongside providing an improvement to their pharmacological properties. The synthesized compounds were evaluated for GSK-3β inhibitory activities, inhibitions of the CXXC5-Dvl interaction, and Wnt-reporter activities to identify dual-targeting inhibitors for more efficient activation of Wnt/β-catenin signaling.

2. Results and discussion

2.1. Strategies and chemistry

6-bromoindirubin-3′-oxime (BIO) is known as a potent inhibitor of GSK-3β, compared with 6-bromoindirubin and indirubin-3′-oxime (IC_{50} of BIO, 6-bromoindirubin and indirubin-3′-oxime on GSK-3 was 5, 45, and 22 nM, respectively) [20]. Whilst in a docking study, the inhibitory activities of these compounds on GSK-3 correlate with their binding energies of GSK-3β in a docking study (binding energy of BIO, 6-bromoindirubin, and indirubin-3′-oxime on GSK-3β were −123.10, −106.73, and −121.16 kcal/mol, respectively, Table 3). Compared to indirubin, the oxime group of I3O could interact with the additional hydrogen bond at L062 of GSK-3β (Fig. 2A and 2B). The Bromo group on 5-bromoindirubin and 6-bromoindirubin also could stabilize a binding mode through additional interactions with amino acids (V070 and C199 on 5-position; K085, L132, and C199 on 6-position) of GSK-3β (Fig. 2C and 2D). Based on these data, various functional groups at the 5- or 6-position could be introduced such as Br, CH_3, CF_3, and OCF_3 groups. The metabolism by an organism is one of the most important determinants of the pharmacokinetic profile of a drug [23]. In vitro microsomal stability assays are widely used in drug discovery. Such assays are based on research involving drug-like compounds, which are cleared predominantly by cytochrome P450 metabolism [24]. The oxime functional group could be susceptible to a reduction by microsomes [25]. Therefore, indirubin-3′-alkoxime derivatives were designed and synthesized to improve microsomal stability.

The 5- or 6-substituted indirubin derivatives **1a-h** were synthesized from the conjugate reaction of 3-indoxyl acetate with various 5- or 6-substituted isatins. Hydrochloric acid (HCl) in ethanol was used at reflux to yield the 5- or 6-substituted indirubin-3′-oxime derivatives **2a-g,** followed by the reaction with hydroxylamine to convert the ketone to

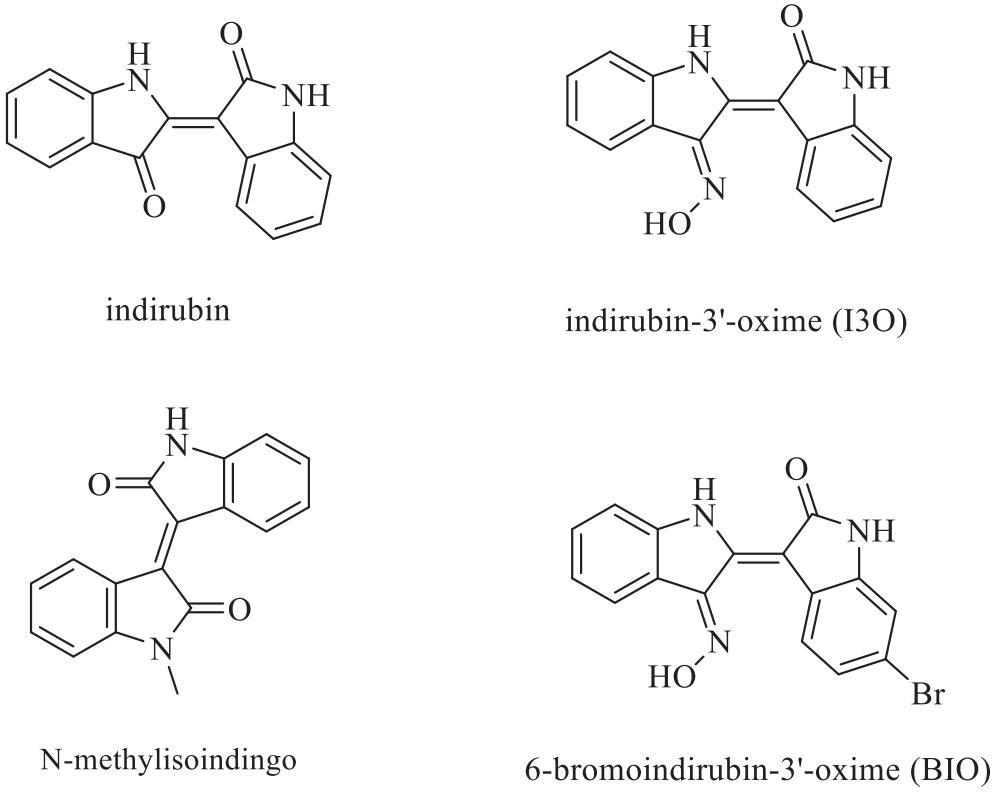

Fig. 1. Chemical structures of indirubin derivatives.

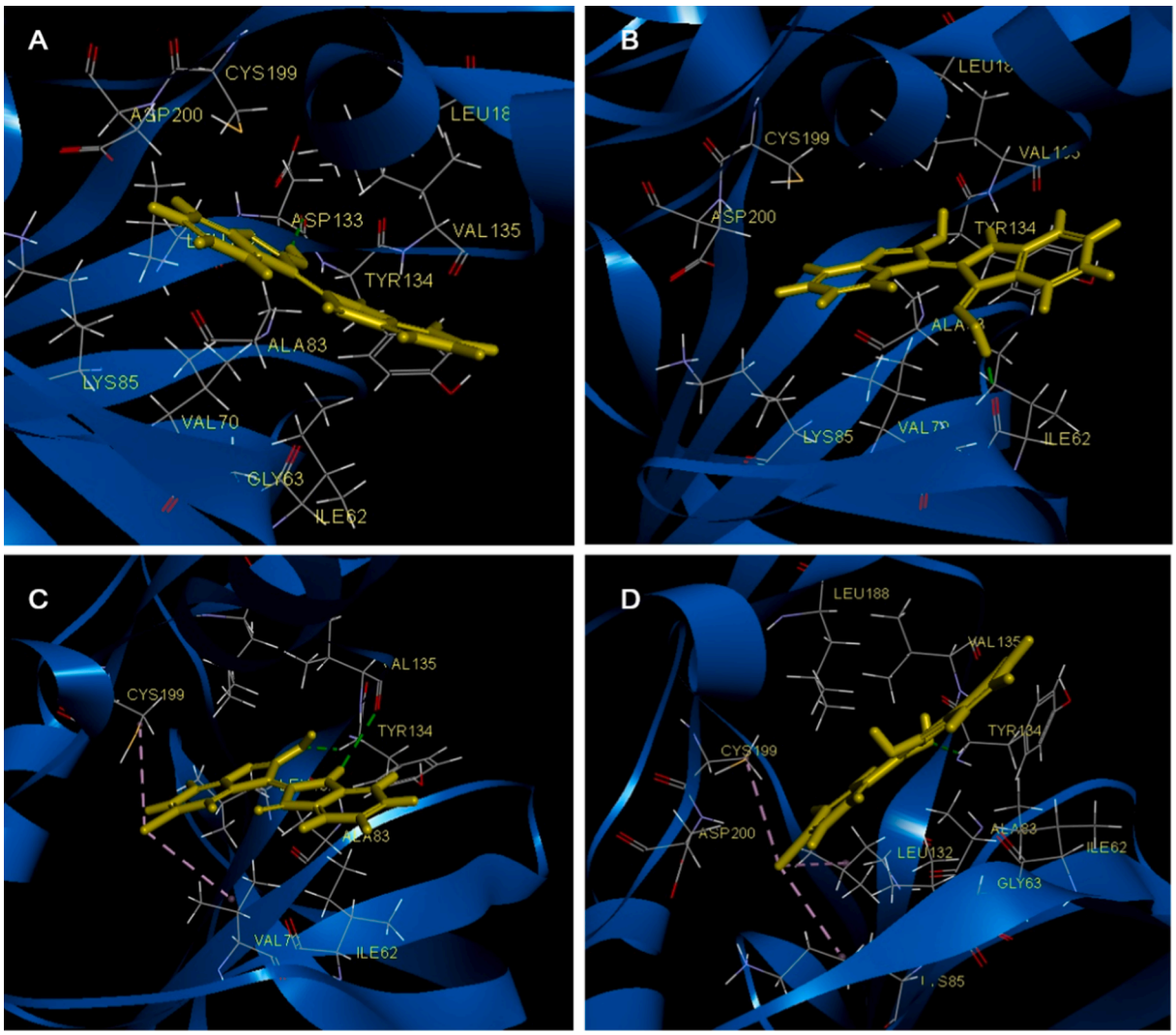

Fig. 2. The binding mode of indirubin derivatives on GSK-3β (PDB ID: 1UV5). A: indirubin, B: indirubin-3′-oxime, C: 5-Br indirubin, D: 6-Br indirubin. (green: hydrogen bond, pale pink: halogen-alkyl interaction).

an *N*-oxime. The 5- or 6-substituted indirubin-3′- alkoxime derivatives **3a-c, 4a-c, 5a-c, 6a-c**, **7a-c**, and **8a-c** were synthesized with *O*-methyl, *O*-ethyl, *O*-propyl, *O*-isopropyl, *O*-isobutyl, and *O*-benzyl hydroxylamine instead of using hydroxylamine and the same procedure as the oxime synthesis. (Scheme 1)

2.2. Inhibition of GSK-3β

Firstly, the synthesized compounds were evaluated for inhibition of GSK-3β (as values of IC_{50}, Table 1). The majority of the compounds exhibited reasonable inhibitory activities towards GSK-3β, except **7a** and **8b**. Both 5-bromoindirubin-3′-oxime and BIO showed excellent inhibitions of GSK-3β (IC_{50} = 4 nM and 4 nM, respectively), while 5-CF_3 indirubin-3′-oxime (IC_{50} = 2 nM) inhibited GSK-3β activities better than BIO. Comparison of the same functional set on the R_1 group among the 5- or 6-substituted indirubin-3′-oxime derivatives, the 5-substituted analogs generally displayed the better inhibitory activities ($R_1 = CH_3$, **2a** and **2e**; $R_1 = CF_3$, **2b** and **2f**; $R_1 = OCF_3$, **2c** and **2 g**). Since three oxime derivatives (R_1 = 5-Br, **2d**; R_1 = 6-Br, BIO; R_1 = 5-CF_3, **2f**) showed outstanding inhibitory activities, their 3′-alkoxime derivatives were prepared at the 3′-oxime position (R_2 groups, **3a-8c**). Among these compounds, all 5-CF_3 indirubin-3′-alkoxime derivatives (**3-8a**) showed excellent inhibitory activities (lower than 20 nM of IC_{50} values). By comparing the R_2 groups of 5- and 6-bromoindirubin-3′-alkoxime derivatives, the larger group displayed lower IC_{50} values (methyl > ethyl > isopropyl > propyl > isobutyl ≈ benzyl group). Among the synthesized compounds, **2f** (R_1 = 5-CF_3 and R_2 = H) and **6c** (R_1 = 5-CF_3 and R_2 = isopropyl) exhibited the most potent inhibitory activity of GSK-3β (2 nM of IC_{50} value).

2.3. Inhibition of the CXXC5-Dvl interaction and activation of Wnt/β-catenin signaling

CXXC5 is a negative modulator of Wnt/β-catenin signaling through its interaction with Dvl in the cytosol [10,11]. The disruption of the CXXC5-Dvl interaction could maintain the activity of Dvl, which negatively modulates GSK-3β. Thus, inhibition of the CXXC5-Dvl interaction suggests that the function of Dvl and Wnt signaling could be preserved. To observe the inhibition of the CXXC5-Dvl interaction by the synthesized compounds, a fluorescence assay was implemented that uses the FITC-conjugated PolyR-DBM. Therefore, by comparing our compounds with a synthesized competitor peptide known to bind with Dvl [10], we can compare their binding to a purified recombinant Dvl PDZ domain. The DBM peptide has been identified from the CXXC5 protein and is a 13-amino acid residue containing an RKTGHQICKFRKC sequence in the zinc finger domain. The well containing the compounds with a Dvl PDZ domain results in a decrease in fluorescence intensity [26]. Thus, the synthesized compounds were evaluated for their cellular inhibitory

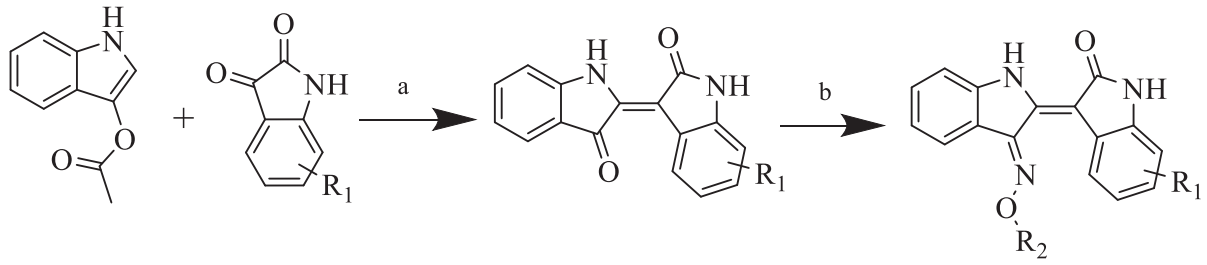

1 **2 ~ 8**

1a R_1 = 6-Br (I)
1b R_1 = 6-CH_3 (II)
1c R_1 = 6-CF_3 (III)
1d R_1 = 6-OCF_3 (IV)
1e R_1 = 5-Br (V)
1f R_1 = 5-CH_3 (VI)
1g R_1 = 5-CF_3 (VII)
1h R_1 = 5-OCF_3 (VIII)

2a-g R_2 = H, R_1 = (II ~ VIII)
3a-c R_2 = methyl, R_1 = (I, V, VII)
4a-c R_2 = ethyl, R_1 = (I, V, VII)
5a-c R_2 = propyl, R_1 = (I, V, VII)
6a-c R_2 = isopropyl, R_1 = (I, V, VII)
7a-c R_2 = isobutyl, R_1 = (I, V, VII)
8a-c R_2 = benzyl, R_1 = (I, V, VII)

Scheme 1. General procedure for synthesis of indirubin-3′-oxime and indirubin-3′-alkoxime analogues. Reagents: (a) HCl, EtOH, reflux; (b) R_2-ONH_2·HCl, pyridine, reflux.

Table 1
Results of biological assays. GSK-3β inhibitory activity, percentage of inhibition on CXXC5-Dvl interaction, and luciferase activity for Wnt reporter assay by synthesized indirubin-3′-oxime and indirubin-3′-alkoxime analogs. (* IC_{50} value of GSK-3β from a previous study [40]).

Cpd	R_1	R_2	GSK-3β, IC_{50} (μM)	Inhibition of CXXC5-Dvl interaction (%)			Wnt reporter assay		
				0.5 μM	1 μM	5 μM	0.5 μM	1 μM	5 μM
indirubin	**H**	**–**	**0.600***		**28**	**28**		**272**	**253**
I3O	**H**	**H**	**0.022***		**4**	**32**		**435**	**701**
BIO	**6-Br**	**H**	**0.004**	**74**	**80**	**94**	**1241**	**4000**	**4439**
2a	**6-CH_3**	**H**	**0.555**		**69**	**81**		**354**	**268**
2b	**6-CF_3**	**H**	**0.144**		**39**	**53**		**389**	**43**
2c	**6-OCF_3**	**H**	**0.338**		**61**	**66**		**336**	**167**
2d	**5-Br**	**H**	**0.004**	**72**	**76**	**90**	**226**	**538**	**5473**
2e	**5-CH_3**	**H**	**0.062**		**79**	**80**		**225**	**1451**
2f	**5-CF_3**	**H**	**0.002**		**15**	**28**		**184**	**2089**
2 g	**5-OCF_3**	**H**	**0.044**		**57**	**55**		**141**	**155**
3a	**6-Br**	**methyl**	**0.026**		**66**	**76**		**979**	**1962**
3b	**5-Br**	**methyl**	**0.028**		**94**	**99**		**335**	**1832**
3c	**5-CF_3**	**methyl**	**0.004**	**55**	**71**	**90**	**2124**	**5093**	**6692**
4a	**6-Br**	**ethyl**	**0.068**		**70**	**85**		**226**	**659**
4b	**5-Br**	**ethyl**	**0.033**	**82**	**78**	**76**	**544**	**584**	**3803**
4c	**5-CF_3**	**ethyl**	**0.006**		**52**	**79**		**4785**	**1576**
5a	**6-Br**	**propyl**	**0.123**		**66**	**19**		**237**	**366**
5b	**5-Br**	**propyl**	**0.121**		**73**	**73**		**185**	**214**
5c	**5-CF_3**	**propyl**	**0.004**		**70**	**87**		**3913**	**2939**
6a	**6-Br**	**isopropyl**	**0.092**		**57**	**80**		**192**	**414**
6b	**5-Br**	**isopropyl**	**0.071**		**66**	**74**		**173**	**531**
6c	**5-CF_3**	**isopropyl**	**0.002**	**68**	**71**	**88**	**1453**	**4127**	**67**
7a	**6-Br**	**isobutyl**	**>3**		**68**	**79**		**236**	**240**
7b	**5-Br**	**isobutyl**	**0.110**		**88**	**92**		**169**	**269**
7c	**5-CF_3**	**isobutyl**	**0.012**	**79**	**86**	**94**	**270**	**411**	**4749**
8a	**6-Br**	**benzyl**	**0.110**		**59**	**82**		**220**	**219**
8b	**5-Br**	**benzyl**	**>3**		**68**	**79**		**158**	**155**
8c	**5-CF_3**	**benzyl**	**0.018**	**67**	**78**	**93**	**107**	**175**	**4061**

activities of CXXC5 binding to Dvl (Table 1). The analogs, which had excellent inhibitory activities of GSK-3β such as BIO, **2d**, **3b-c**, **5c**, **6c**, **7c**, and **8c** presented an inhibition of these protein–protein interactions of over 85 % at 5 μM. However, **2f** did not inhibit the interaction between CXXC5 and Dvl, although it had previously provided an excellent IC_{50} value on GSK-3β. Many of the compounds displaying an IC_{50} value of GSK-3β, at approximately 100 nM or greater, exhibited insufficient inhibitory activities towards the interaction between CXXC5 and Dvl (**2a-c**, **5b**, **6a-b**, **7a**, and **8a-b**) Compounds that presented < 70 % inhibition of the CXXC5-Dvl interaction (**2b**, **2c**, **2f**, and **2 g**) were all oxime derivatives and similarly, did not increase the Wnt activation irrespective of the GSK-3β inhibitory activity. Mainly, the 5-CF_3 substituted indirubin-3′-alkoxime derivatives exhibited improved inhibitory activities on the interaction between CXXC5 and Dvl, compared to the 5-Br and/or 6-Br substituted indirubin-3′-alkoxime derivatives that contained a relatively bulky group on R_2 (R_2 =

isopropyl, **6a-c**; R_2 = isobutyl, **7a-c**; R_2 = benzyl, **8a-c**).

Next, a cellular reporter assay used to investigate Wnt activation through analyses of TOPFlash activity was implemented to evaluate all the synthesized compounds in HEK293 reporter cells. The HEK-TOP cells are stable cell lines that consistently express TOPFlash [27]. The compounds displayed a range of Wnt activity levels such as: (43–6692) **2a-c**, **2e**, **2 g**, **4a**, **5a-b**, **6a-b**, **7a-b**, and **8a-b** exhibited very poor Wnt activations (under 1500 at 1 and 5 μM, Table 1). While, BIO, **3c**, **4c**, **5c**, and **6c** induced strong Wnt activation levels at 1 μM. The role of the synthesized compounds in the activation of Wnt/β-catenin signaling was further verified by the increment of β-catenin at 1 μM (BIO, **2d**, **2f**, **3c**, **4c**, **6c**, and **8c**; Fig. 3). Compounds with sufficient Wnt activation at 1 μM increase β-catenin by immunoblot analysis. Indeed, compounds **4c** and **6c** showed higher Wnt activations at 1 μM than 5 μM, possibly caused by increased cellular toxicity (Fig. 4). Comparatively, BIO compounds **2d**, **3c**, **4b**, **7c**, and **8c** induced strong Wnt activation levels over 3800 at 5 μM. Generally, among the 5- or 6-substituted indirubin-3′-oxime derivatives, 5-substituted indirubin-3′-oximes mostly displayed higher Wnt activity levels at 5 μM than 6-substituted indirubin-3′-oximes by comparison of R_1 group (R_1 = Br, BIO and **2d**; R_1 = CH_3, **2a** and **2e**; R_1 = CF_3, **2b** and **2f**; R_1 = OCF_3, **2c** and **2 g**). Most of the 5-CF_3 indirubin-3′-alkoxime derivatives (**3-4c** and **6-8c**) showed notable Wnt activation levels, with **3c** (R_1 = 5-CF_3 and R_2 = methyl) the most significant Wnt activator among these series.

2.4. Cell cytotoxicity assay

Potent GSK-3β inhibitors can induce cell death at high concentrations [28]. In this study, the cell viability after administering the compounds was measured by MTT assay. Indeed, all of the tested compounds did not demonstrate increased toxicity at 1 μM (BIO, **2f**, **4b**, **4c**, **6c**, **7c**, and **8c**; Fig. 4). However, most of the compounds that elicit a strong inhibition of GSK-3β (IC_{50} < 10 nM; BIO, **4c**, and **6c**) exhibited cell cytotoxicity at 5 and 10 μM. This increased cytotoxicity may provide an explanation as to why **4c** and **6c** were more active at 1 μM compared with 5 μM in the Wnt-reporter assay (Table 1). Instead, **4b**, which provides less potent inhibition of GSK-3β (IC_{50} > 30 nM) did not show cytotoxicity despite their sufficient activation of Wnt signaling. Thus, the strong GSK-3β inhibitors possibly cause cytotoxicity and may reduce the activation of Wnt signaling at high concentrations.

2.5. Relationship of Wnt/β-catenin signaling with GSK-3β and CXXC5-Dvl interaction

Inhibition of GSK-3β-mediated β-catenin phosphorylation is known to be the key event in Wnt/β-catenin signalling [29]. Interestingly, a peptide that competitively inhibits the CXXC5-Dvl interaction is capable of alleviating CXXC5-mediated inhibition of Wnt signalling [10,11]. Thus, we examined the relationships of Wnt activation with dual inhibition of GSK-3β and the CXXC5-Dvl interaction. The compounds that

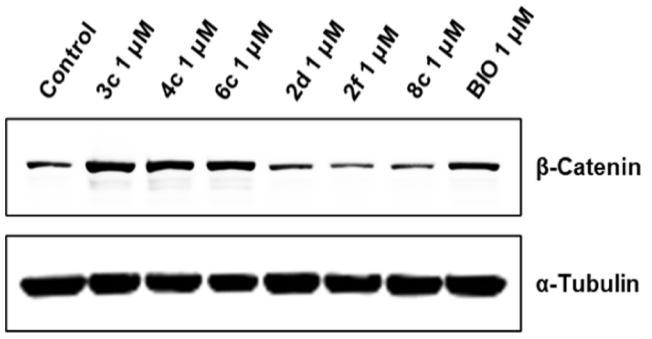

Fig. 3. Immunoblot analyses with the indicated antibodies in HEKTOP cells treated with synthesized compounds at 1 μM for 24 h.

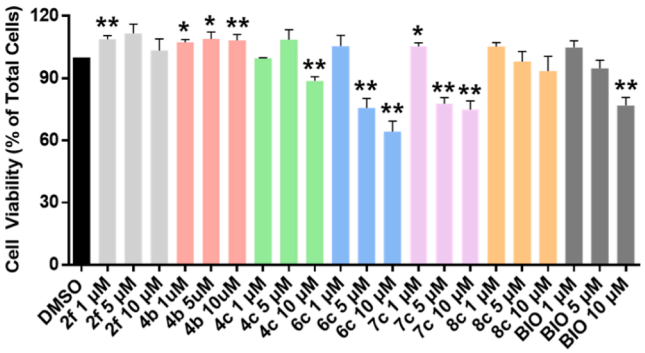

Fig. 4. Evaluation of cell cytotoxicity by MTT assay at 1, 5, and 10 μM of compounds. (*$p < 0.05$; **$p < 0.01$ compared with DMSO control).

had an IC_{50} higher than 40 nM against GSK-3β (**2a-c**, **2e**, **2g**, **4a**, **5a-b**, **6a-b**, **7a-b**, and **8a-b**) demonstrated relatively low Wnt activation, independently of their ability to disrupt the interaction between the CXXC5-Dvl proteins. The compounds providing < 70 % inhibition of the CXXC5-Dvl interaction (**2b**, **2c**, **2f**, and **2g**) are oxime derivatives and likewise did not increase Wnt activation, regardless of their GSK-3β inhibitory activity. Indeed, **7b** which has an IC_{50} of 110 nM against GSK-3β and severely inhibits the CXXC5-Dvl interaction (> 90 % inhibition at 5 μM) also did not activate Wnt signaling. Alternatively, **2f** which has an excellent inhibitory activity of GSK-3β (2 nM of IC_{50} on GSK-3β inhibition), while only providing a poor inhibition of the CXXC5-Dvl interaction, also did not show sufficient activation of Wnt signaling. However, **2d**, **3c**, **6c**, **7c**, **8c**, and BIO, in the Wnt-reporter assay all illustrated readouts greater than 4,000 at 5 μM (Table 1), alongside most showing lower than 20 nM of IC_{50} on GSK-3β, and a higher than 88 % inhibition of the interaction between CXXC5-Dvl proteins at 5 μM. Thus, we assume that activation of Wnt signaling seems to inhibit both GSK-3β and the CXXC5-Dvl interaction, whereas extremely strong inhibition of GSK-3β could induce cytotoxicity at high concentrations. Thereby, dual inhibition of GSK-3β and the CXXC5-Dvl interaction seems to be a better approach for safely and efficiently activating the Wnt signal compared to inhibiting GSK-3β alone.

2.6. Docking study

For monitoring the binding modes of **6c**, **7c**, and **8c**, which showed effective inhibition of both GSK-3β and the CXXC5-Dvl interaction, the molecular docking studies were performed at the ATP binding site of GSK-3β (PDB ID: 1UV5) [20] and the PDZ domain of Dvl (PDB ID: 2KAW [30] and 6LCB).

These compounds were bound in the narrow tubular hydrophobic pocket of GSK-3β. Both **6c** and **7c** displayed a similar binding mode with BIO, which possesses a hydrogen bond with V135 and P136 on the amide group of isatin (Fig. 5A and 5B). In addition, the functional groups of **6c** and **7c** provided extra stabilization at the 5-position (R_1 = CF_3) through pi–alkyl interactions or hydrogen bonds with V110, L132, C199, and D200. Likewise, on 3′-position (R_2 group) by pi–alkyl interactions with V070 through stable binding in the narrow hydrophobic pocket (Figure 5 and S1). **8c** showed a different binding mode from **6c** and **7c** because of the bulky benzyl group at the 3′-oxime position: the amide group of isatin formed a hydrogen bond with D200 instead of V135 and P136 (Fig. 5C), and the functional groups at the 5-position interacted with Q185 instead of V110 and L132 at the 5-position (Figure S1). The benzyl group at the 3′-position of **8c** also stabilized binding through additional interaction with I062 (Figure S1). Notwithstanding their binding modes, **6c**, **7c**, and **8c** each properly fitted in GSK-3β and showed reasonable binding energies alongside BIO.

Dishevelled (Dvl) plays a vital role in Wnt signaling and its PDZ domain interacts with membrane receptors and downstream molecules

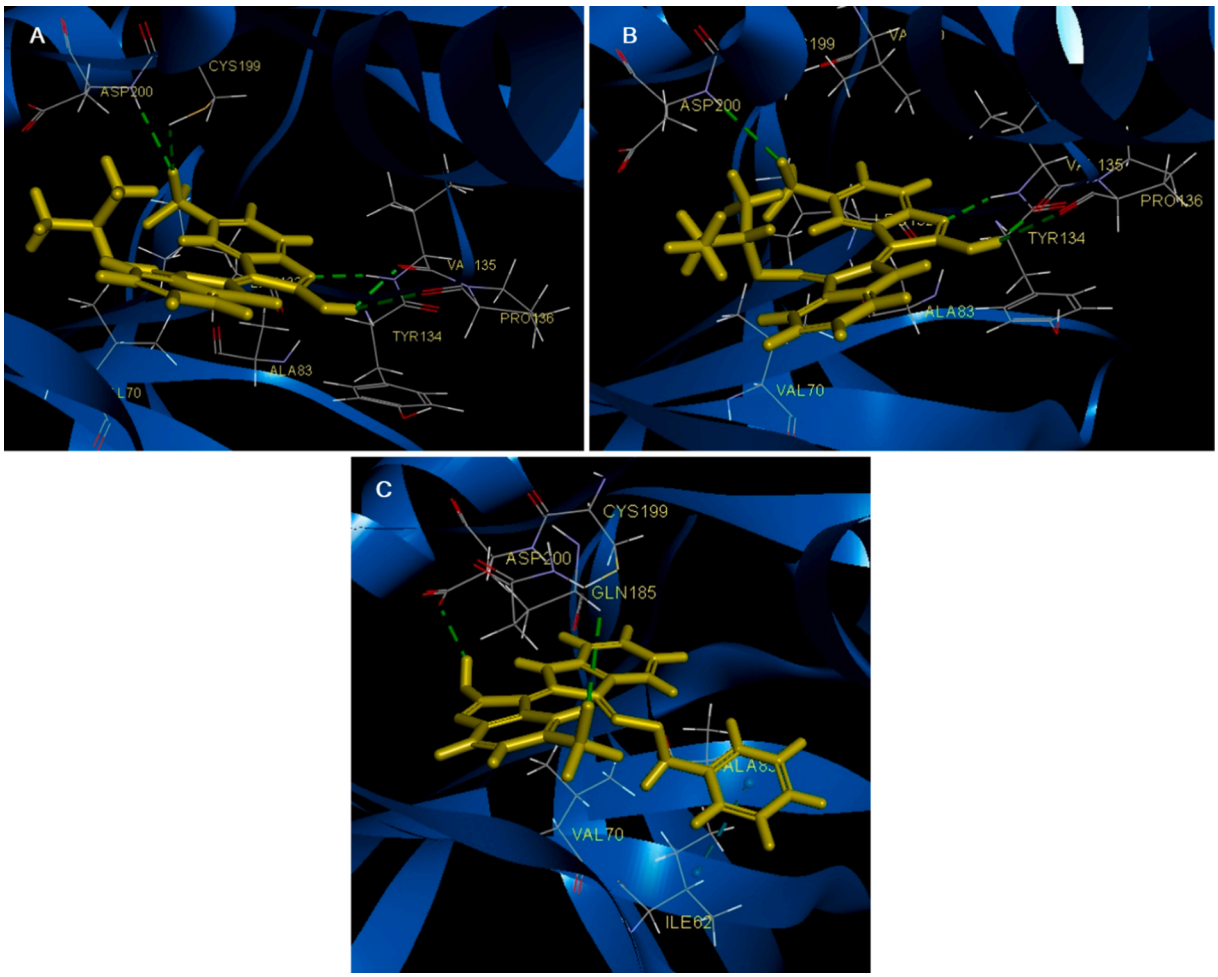

Fig. 5. The binding mode of indirubin-3′-alkoxime derivatives on GSK-3β (PDB ID: 1UV5). A: **6c**, B: **7c**, C: **8c**. (green: hydrogen bond).

[31]. CXXC5 is one of the key molecules that interact with Dvl and negatively regulates the Wnt/β-catenin pathway [10]. A Dvl binding motif (DBM peptide, residue 279–291, RKTGHQICKFRKC) was identified in the C-terminal region of CXXC5. Disruption of the CXXC5-Dvl interaction by the DBM peptide activated the Wnt/β-catenin signaling pathway [32]. Residues I264, I266, V318, L321, and V325 of the Dvl PDZ formed a hydrophobic binding pocket, and I285 of the DBM peptide was well accommodated into the pocket [33]. As indole derivatives are known to interact with the PDZ domain [21], structurally similar BIO and I3O could also interact with the PDZ domain (PDB ID: 2KAW) of the Dvl protein in an in silico docking model [22]. In this study, CXXC5, **6c**, **7c**, and **8c** bound to the PDZ domain of Dvl (2KAW) by pi–alkyl interactions or forming hydrogen bonds with I264, I266, V318, and/or V325 and by van der Waals interactions with L321 (Fig. 6 and S2). R322, which is critical for ligand binding with the PDZ domain through hydrogen bond formation [30], also interacted with a 5-CF_3 group of these compounds by a hydrogen bond. The inhibitory activity of the CXXC5-Dvl interaction on **6c**, **7c**, and **8c** (71, 86, and 78 % inhibition at 1 μM, respectively) were well correlated with their binding energies (−119.63, −124.79, and −121.10 kcal/mol, respectively). (Table 1 and 3). As a result, these 3 compounds were well bound to the PDZ domain of Dvl as well as to GSK-3β.

2KAW in PDB is an NMR structure of the mouse's Dvl1 PDZ domain, and 6LCB in PDB is a crystal structure of the human's Dvl1 PDZ domain. Sequences of these two Dvl1 PDZ domains are nearly identical, sharing 100 % of sequence similarity and 98 % sequence identity (Fig. S3). Furthermore, the root mean square deviation (RMSD) of these two proteins was calculated for the structural similarity. The RMSD value of the global backbone is distributed around 1.75 Å by C-alpha pairs, which were useful for both building and validating models of protein structure [34]. The RMSD value of the binding sites is distributed around 1.17 Å by tethering amino acids of each structure. Based on the RMSD values, the binding sites of these two proteins seem to be more similar than the whole structure. For this reason, there are no significant differences in the docking results for the two structures (Figs. 6 and 7). **6c**, **7c**, and **8c** were docked onto the binding site of the PDZ domain (PDB ID: 6LCB) and interacted with residues L262, G263, I264, I266, V318, L321, R322, and V325 in the PDZ domain of the Dvl protein, like a binding mode with a 2KAW structure (Fig. 7 and Fig. S4). Additionally, the simulated docking mode of the synthesized compounds was similar to the binding mode of the original ligand (NPL3009, PDB ID: E83) on 6LCB (Fig. 8 and Fig. S4D). Collectively, it can be assumed that the series of indirubin-3′-alkoxime derivatives bind to the Dvl protein.

2.7. Metabolic stability on microsome and plasma

Metabolic stability is very important in monitoring the pharmacokinetic profile. The metabolic stability profiles of five active analogs (**2d**, **3c**, **4b**, **6c**, **7c**, and **8c**) that showed excellent Wnt activation, were evaluated on human liver microsome and plasma (Table 2). All 5 analogs were stable at over 89 % for 30 min or over 97 % at 60 min on plasma. In NADPH-dependent cytochrome P450 (CYP450) conditions, **4b** showed remarkable microsomal stability, showing 85.5% remaining for 30 min, while **6c**, **7c**, and **8c** showed enhanced microsomal stability with 99.1 %, 98.7 %, and > 10 0% remaining at 60 min, respectively. All these analogs showed higher microsomal stability than **2d**, **3c**, and BIO,

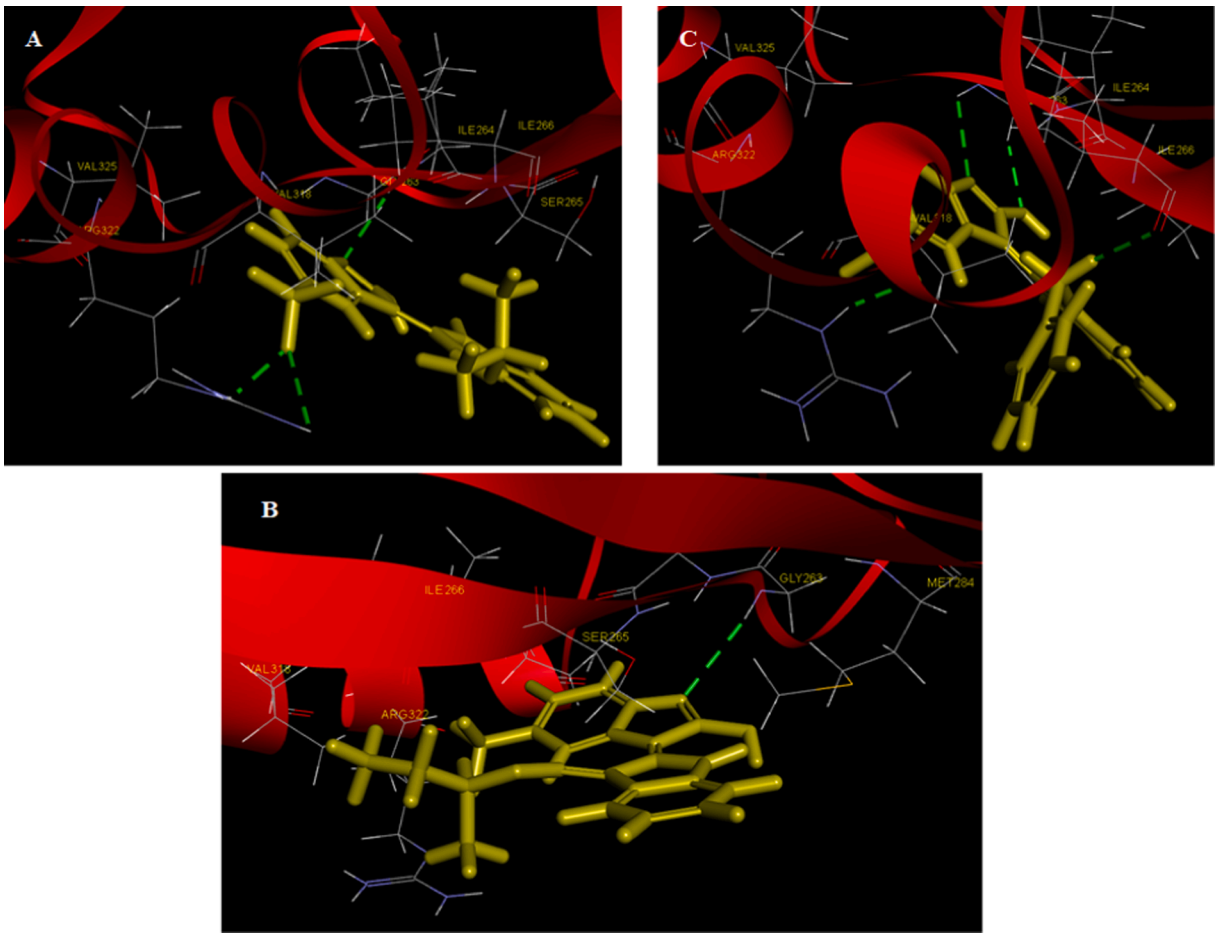

Fig. 6. The binding mode of indirubin-3′-alkoxime derivatives on PDZ domain of Dvl (PDB ID: 2KAW). A: **6c**, B: **7c**, C: **8c**. (green: hydrogen bond).

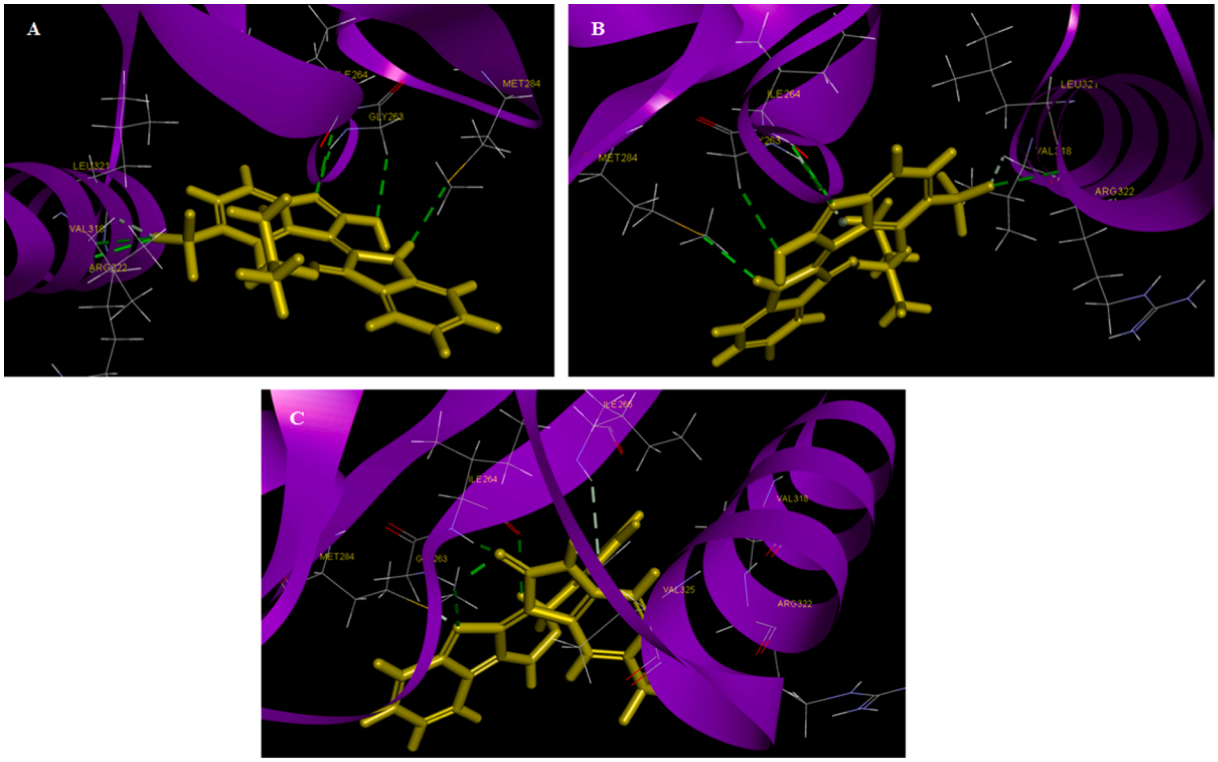

Fig. 7. The binding mode of indirubin-3′-alkoxime derivatives on PDZ domain of Dvl (PDB ID: 6LCB). A: **6c**, B: **7c**, C: **8c**. (green: hydrogen bond).

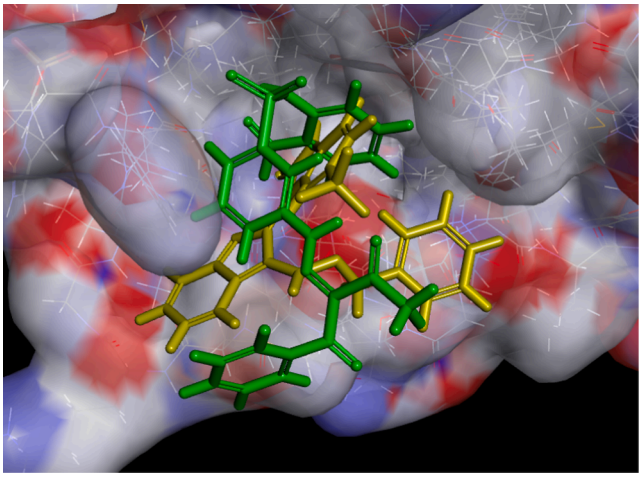

Fig. 8. The docking mode of **8c** (yellow) and NPL3009 (green) in Dvl protein (PDB ID: 6LCB).

Table 2
Microsomal and plasma stability of indirubin-3′-oxime and indirubin-3′-alkoxime derivatives.

Cpd	R_1	R_2	Microsomal stability (human, % remaining)		Plasma stability (human, % remaining)		
			30 min[a]	60 min[b]	30 min[c]	60 min[d]	120 min[c]
BIO	6-Br	H	37.3		91.7		84.8
2d	5-Br	H	53.9		94.3		94.2
3c	5-CF_3·HCl	methyl	59.4		95.9		87.0
4b	5-Br	ethyl	85.5		97.8		83.1
6c	5-CF_3·HCl	isopropyl	>100	99.1	89.2		83.7
7c	5-CF_3·HCl	isobutyl		98.7		97.1	
8c	5-CF_3·HCl	benzyl		>100		>100	

a Microsomal stability method 1 , c. Plasma stability method 1.
b Microsomal stability method 2 , d. Plasma stability method 2.

Table 3
The binding energy of indirubin, indirubin-3′-oxime, and indirubin-3′-alkoxime derivatives.

Cpd	Binding energy (kcal/mol)		
	1UV5	2KAW	6LCB
BIO	−123.10		
indirubin	−103.05		
indirubin-3′-oxime	−121.16		
5-bromo indirubin	−121.42		
6-bromo indirubin	−106.73		
6c	−151.14	−119.63	−106.72
7c	−151.85	−124.79	−106.99
8c	−173.08	−121.10	−101.72

which exhibited only moderate microsomal stability (53.9 %, 59.4 %, and 37.3 % remaining at 30 min, respectively). By comparing R_2 groups, compounds containing a larger substituent were more stable on the microsome (H < methyl ≪ ethyl < isopropyl ≈ isobutyl ≈ benzyl group). Overall, the analogs with 3′-alkoxime displayed higher stability against microsomal enzymes than the analogs with 3′-oxime.

2.8. In vitro migration assay for wound healing

The Wnt/β-catenin signaling pathway is activated during the wound healing process [35]. GSK-3β inhibitors induce cutaneous wound healing, dermal fibrosis and enhance migration of HaCaT keratinocytes by activation of the Wnt/β-catenin pathway [16,36,37]. Also, combination treatment of skin wounds with PTD-DBM, a peptide blocking the CXXC5-Dvl interaction, and a GSK-3β inhibitor that activates the Wnt/β-catenin pathway, synergistically enhance cutaneous wound healing in mice [16]. To monitor the effects of 3′-alkoxime derivatives on wound healing and avoid a cell cytotoxicity issue, indirubin, I3O, BIO, **4b**, **6c**, **7c**, and **8c** were evaluated with HaCaT keratinocyte migration after scratch wounding at 1 μM (Fig. 9). Indirubin itself promotes the migration of keratinocytes [38], but BIO delays the migratory activity of fibroblasts due to its cytotoxicity [39]. Therefore, 24 h after treatment of 1 μM of the compounds, **6c**, indirubin, and I3O all showed limited wound healing activities with a HaCaT keratinocytes migration assay. **8c** and I3O induced slightly better wound healing activity (68 % and 64 %, respectively, compared to 60 % for the control). **4b** and **7c** enhanced narrowing of the scratch wound (74 % and 82 %, respectively, relative wound healing rate). To confirm that the effect of wound healing is through activation of Wnt signaling, indirubin, I3O, BIO, **4b**, **6c**, **7c**, and **8c** were evaluated on Wnt activation in HaCaT cells using immunocytochemical analysis (Fig. 10). Subsequently, 24 h after 1 μM treatment of compounds **4b**, **6c**, **7c**, and **8c**, total β-catenin levels and nuclear translocation of β-catenin increased. These compounds also showed the correlation of their Wnt activation in HaCaT cells with their migration of keratinocytes. Therefore, these compounds could promote wound healing by activating Wnt/β-catenin signaling. Also, the results of wound healing were correlated against Wnt activation using a cellular reporter assay at 5 μM except for BIO. Most of our compounds promoted keratinocyte migration much better than indirubin or I3O. Although **4b** could be efficient at high concentration with respect to the cytotoxicity, **7c** could be a potential candidate for wound healing through activation of the Wnt/β-catenin signaling pathway, through dual inhibition of GSK-3β and the CXXC5-Dvl interaction.

3. Discussion

GSK-3β inhibitors effectively promote Wnt signaling. However, these could have a limitation because of the negative Wnt regulator such as CXXC5. So, dual inhibition of the CXXC5–Dvl interaction and GSK-3β seems to be efficient for activating Wnt/β-catenin signaling. In previous studies, both Indirubin and BIO were reported as selective inhibitors of GSK-3β and were found to interact with the PDZ domain of Dvl [33].

Here, a series of indirubin-3′-oxime and 3′-alkoxime derivatives, with various functional groups at the 5- or 6-position, were prepared to improve the biological potency and the pharmacokinetic profile. Twenty-five analogs were synthesized through the introduction of Br, CH_3, CF_3, and OCF_3 groups on the 5- or 6- position (R_1 group) and alkyl or benzylic moieties on the 3′-oxime position (R_2 group). Among the synthesized indirubin-3′-oximes, three oxime derivatives (R_1 = 5-Br, 6-Br, and 5-CF_3) showed remarkable inhibitory activities against GSK-3β. All 5-CF_3 indirubin-3′-alkoxime derivatives also displayed excellent inhibitory activities against GSK-3β. By comparing R_2 groups of 5- and 6-bromoindirubin-3′-alkoxime derivatives, the bigger group showed lower IC_{50} values of GSK-3β. In general, 5-CF_3 substituted indirubin-3′-alkoxime derivatives exhibited better inhibitory activities on the interaction between CXXC5 and Dvl than 5-Br and/or 6-Br substituted indirubin-3′-alkoxime derivatives, which contained a relatively bulky group on R_2. In regards to the Wnt-reporter assay, among 5- or 6-substituted indirubin-3′-oxime derivatives, 5-substituted indirubin-3′-oximes generally displayed higher Wnt activation at 5 μM than 6-substituted indirubin-3′-oximes by comparison of the R_1 group. Most of the 5-CF_3 indirubin-3′-alkoxime derivatives induced remarkable Wnt activation levels. In the MTT assay, some indirubin-3′-alkoxime derivatives with strong GSK-3β

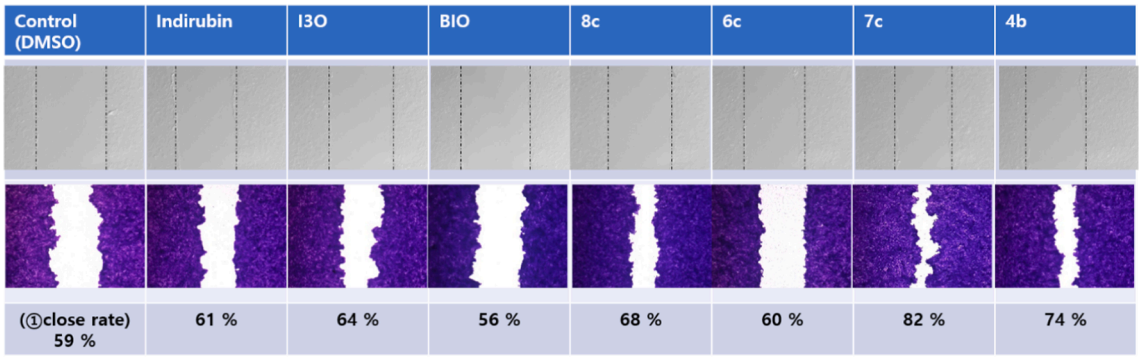

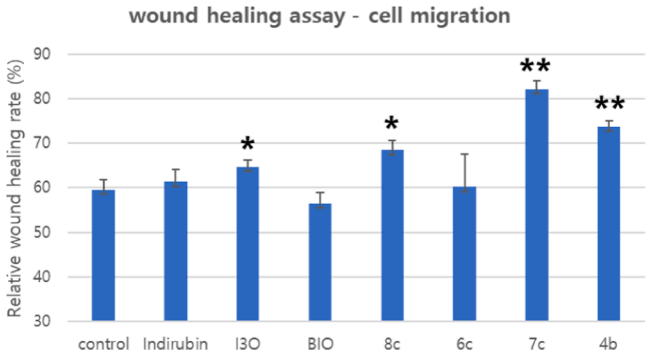

Fig. 9. The effects on migration of HaCaT cells through in vitro wound-healing assay at 1 μM. The wound healing rate was measured by the Image J program ($n = 3$). Indirubin, I3O, BIO, **4b**, **6c**, **7c**, and **8c** as indirubin-3′-alkoxime derivatives were evaluated on cell migration compared to DMSO. $*p < 0.5$,$**p < 0.05$.

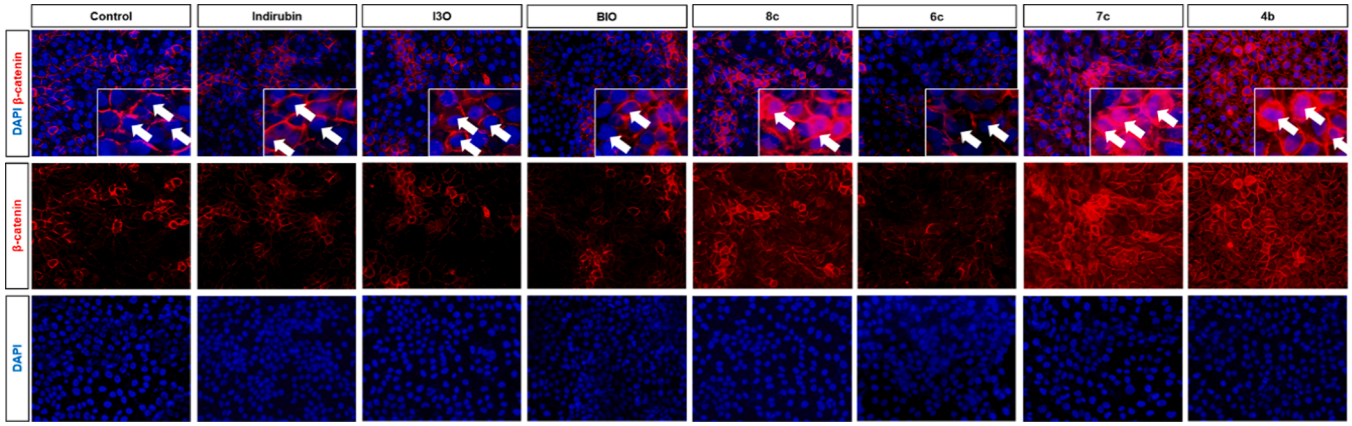

Fig. 10. The effects on Wnt activation in HaCaT cells. HaCaT cells were treated with indirubin, I3O, BIO, **4b**, **6c**, **7c**, and **8c** (1 μM) for 24 h. Fixed cells were stained for immunocytochemical analysis with an anti-β-catenin antibody (red) and DAPI (blue). Arrows indicate nuclei.

inhibitory activity cause cytotoxicity at high concentration, even though at low concentration, these could increase β-catenin expression and Wnt activation. Strong GSK-3β inhibition could reduce activation of Wnt signaling and induce cell death at high concentrations. Based on in vitro analyses such as GSK-3β inhibitory activities, inhibition of the CXXC5-Dvl interaction, and Wnt-reporter activities, the inhibition of both GSK-3β and CXXC5-Dvl interaction were crucial factors in controlling Wnt signaling. Indeed, only extremely potent inhibition of GSK-3β led to cytotoxicity at high dosage concentrations. In a docking study, indirubin-3′-alkoxime derivatives were well bound in GSK-3β and the Dvl-PDZ domain and exhibited reasonable binding energies. Especially, these were docked onto the binding site of the Dvl-PDZ domain, like CXXC5, and interacted with residues of I264, I266, V318, L321, and V325 in the binding site. Collectively, a series of indirubin-3′-alkoxime derivatives are suggested to bind the Dvl protein. Metabolic stability profiles of six active analogs (**2d**, **3c**, **4b**, **6c**, **7c**, and **8c**), which showed excellent Wnt activation, were evaluated in human liver microsome and plasma. All of these compounds were stable in plasma. Compounds with 3′-alkoxime (**4b**, **6c**, **7c**, and **8c**) showed impressive increases in microsomal stability compared with compounds with 3′-oxime (BIO, **2d**, and **3c**). By comparing R_2 groups, compounds with the bigger group were more stable in microsome studies. To evaluate the effects of 3′-alkoxime derivatives on wound healing, **4b**, **6c**, **7c**, and **8c** were evaluated on HaCaT keratinocyte migration after scratch wounding and on Wnt activation of HaCaT cells using an immunocytochemical analysis. The results of wound healing activity were relatively correlated with the Wnt activation in HaCaT cells. As such, these derivatives could induce wound healing activity by activating Wnt/β-catenin signaling. Although **4b** could be efficient at high concentrations in aspects of its cytotoxicity, **7c** enhanced narrowing of the scratch wound. In conclusion, dual

inhibition of GSK-3β and the CXXC5-Dvl interaction seems to be a better approach for safely and efficiently activating Wnt/β-catenin signaling compared to inhibiting GSK-3β alone.

4. Experimental section

4.1. Chemistry

All chemicals were obtained from commercial suppliers and used without further purification. All reactions were monitored by thin-layer chromatography on precoated silica gel 60 F254 (mesh) (E. Merck, Mumbai, India), and spots were visualized under UV light (254 nm). Flash column chromatography was performed with silica (Merck EM9385, 230–400 mesh). ^{1}H and ^{13}C nuclear magnetic resonance (NMR) (Agilent Technologies) spectra were recorded at 400 and 100 MHz, respectively. Proton and carbon chemical shifts are expressed in ppm relative to internal tetramethylsilane. Coupling constants (*J*) are expressed in Hertz. Splitting patterns are presented as s, singlet; d, doublet; t, triplet; q, quartet; dd, double of doublets; m, multiplet; br, broad. Liquid chromatography-mass spectrometry (LC-MS) spectra were obtained with an electrospray ionization (ESI) probe using a Shimadzu LCMS-2020 instrument with an Agilent C18 column (50*4.6 mm, 5 μm). The detected ion peaks were *m/z* in a positive and negative scan mode, where M represents the molecular weight of the compound and z represents the charge (number of protons). High-resolution ESI-MS measurements were performed on an Agilent 6530 Accurate-Mass Quadrupole Time-of-Flight (Q-TOF) LC-MS system (Santa Clara, CA, USA) in negative or positive mode. Elemental compositions were determined on Elemental analysis (EA) using a Thermo Scientific FLASH2000 instrument. To determine the purity of the final compounds, HPLC experiments were conducted using an Agilent analytic column eclipse-XDB-C_{18} (150*4.6 mm, 5 μm) on a Shimadzu HPLC-2010 instrument.

4.1.1. General procedure for **1**

Various 5- or 6-substituted isatins were dissolved in ethanol (0.05 M) with 3-indoxyl acetate (1 eq) then hydrochloride (35 %, cat.) was added. The reaction mixture was stirred and refluxed for 8 h. After reacting, the purple precipitate in the terminated reaction mixture was filtered and washed with ethanol (0.05 M) then dried at a vacuum condition.

*4.1.1.1. (Z)-6′-bromo-[2,3′-biindolinylidene]-2′,3-dione **(1a)**.* 6-Bromoisatin (281 mg, 1.24 mmol) and 3-acetoxyindole (218 mg, 1.24 mmol) were used and **1a** (270 mg, 61 %, purple solid) was obtained. ^{1}H NMR (400 MHz, DMSO-d_6) δ 11.07 (d, J = 18.4 Hz, 2H), 8.69 (d, J = 7.6 Hz, 1H), 7.67 (d, J = 6.8 Hz, 1H), 7.60 (t, J = 7.4 Hz, 1H), 7.44 (d, J = 6.4 Hz, 1H), 7.24 (d, J = 7.6 Hz, 1H), 7.06 (br s, 2H). RP-HPLC (254 nm): 96 % (t_R = 12.5 min). LC/MS (ESI, *m/z*) 339 [M−H]$^-$.

*4.1.1.2. (Z)-6′-methyl-[2,3′-biindolinylidene]-2′,3-dione **(1b)**.* 6-Methylisatin (300 mg, 1.86 mmol) and 3-acetoxyindole (326 mg, 1.86 mmol) were used and **1b** (315 mg, 6 %, purple solid) was obtained. ^{1}H NMR (400 MHz, DMSO-d_6) δ 11.02 (s, 1H), 10.82 (s, 1H), 8.63 (s, 1H), 7.64 (d, J = 7.6 Hz, 1H), 7.58 (t, J = 7.8 Hz, 1H), 7.42 (d, J = 8.0 Hz, 1H), 7.08–7.00 (m, 2H), 6.79 (d, J = 7.6 Hz, 1H), 2.32 (s, 3H). RP-HPLC (254 nm): 97 % (t_R = 15.3 min). LC/MS (ESI, *m/z*) 299 [M−H]$^-$.

*4.1.1.3. (Z)-6′-(trifluoromethyl)-[2,3′-biindolinylidene]-2′,3-dione **(1c)**.* 6-Trifluoromethylisatin (246 mg, 1.14 mmol) and 3-acetoxyindole (200 mg, 1.14 mmol) were used and **1c** (276 mg, 73 %, purple solid) was obtained. ^{1}H NMR (400 MHz, DMSO-d_6) δ 11.20 (s, 2H), 8.87 (d, J = 10.8 Hz, 1H), 7.68–7.65 (m, 1H), 7.62–7.57 (m, 1H), 7.45–7.42 (m, 1H), 7.39–7.35 (m, 1H), 7.10–7.03 (m, 2H). RP-HPLC (254 nm): 99 % (t_R = 12.7 min). LC/MS (ESI, *m/z*) 329 [M−H]$^-$.

*4.1.1.4. (Z)-6′-(trifluoromethoxy)-[2,3′-biindolinylidene]-2′,3-dione **(1d)**.* 6-Trifluoromethoxyisatin (264 mg, 1.14 mmol) and 3-acetoxyindole (200 mg, 1.14 mmol) were used and **1d** (127 mg, 29 %, purple solid) was obtained. ^{1}H NMR (400 MHz, DMSO-d_6) δ 11.08 (s, 2H), 8.83 (dd, J = 11.2, 0.4 Hz, 1H), 7.68–7.65 (m, 1H), 7.62–7.56 (m, 1H), 7.44–7.41 (m, 1H), 7.07–6.98 (m, 2H), 6.84–6.82 (m, 1H). RP-HPLC (254 nm): 90 % (t_R = 13.1 min). LC/MS (ESI, *m/z*) 345 [M−H]$^-$.

*4.1.1.5. (Z)-5′-bromo-[2,3′-biindolinylidene]-2′,3-dione **(1e)**.* 5-Bromoisatin (600 mg, 2.66 mmol) and 3-acetoxyindole (465 mg, 2.66 mmol) were used and **1e** (494 mg, 55 %, purple solid) was obtained. ^{1}H NMR (400 MHz, DMSO-d_6) δ 11.10 (s, 2H), 8.94 (d, J = 2.0 Hz, 1H), 7.66 (d, J = 7.2 Hz, 1H), 7.61–7.57 (m, 1H), 7.44–7.39 (m, 2H), 7.07–7.03 (m, 1H), 6.86 (d, J = 8.0 Hz, 1H). RP-HPLC (254 nm): 99 % (t_R = 16.6 min). LC/MS (ESI, *m/z*) 339 [M−H]$^-$.

*4.1.1.6. (Z)-5′-methyl-[2,3′-biindolinylidene]-2′,3-dione **(1f)**.* 5-Methylisatin (500 mg, 3.10 mmol) and 3-acetoxyindole (544 mg, 3.10 mmol) were used and **1f** (582 mg, 68 %, purple solid) was obtained. ^{1}H NMR (400 MHz, DMSO-d_6) δ 10.88 (s, 2H), 8.45 (s, 1H), 7.62 (d, J = 8.0 Hz, 1H), 7.54 (t, J = 6.0 Hz, 1H), 7.37 (d, J = 8.0 Hz, 1H), 6.98 (t, J = 8.0 Hz, 1H), 6.82–6.75 (m, 2H), 3.75 (s, 3H). RP-HPLC (254 nm): 97 % (t_R = 15.3 min). LC/MS (ESI, *m/z*) 277 [M + H]$^+$.

*4.1.1.7. (Z)-5′-(trifluoromethyl)-[2,3′-biindolinylidene]-2′,3-dione hydrochloride **(1g)**.* 5-Trifluoromethylisatin (273 mg, 1.14 mmol) and 3-acetoxyindole (200 mg, 1.14 mmol) were used and **1 g** (289 mg, 61 %, purple solid) was obtained. ^{1}H NMR (400 MHz, DMSO-d_6) δ 12.65 (s, 1H), 11.23 (s, 1H), 11.09 (s, 1H), 9.45 (d, J = 2.4 Hz, 1H), 7.89 (dd, J = 11.2, 2.4 Hz, 1H), 7.69–7.66 (m, 1H), 7.63–7.57 (m, 1H), 7.43 (d, J = 10.4 Hz, 1H), 7.08–7.03 (m, 1H), 6.99 (dd, J = 11.2, 0.8 Hz, 1H). RP-HPLC (254 nm): 88 % (t_R = 5.4 min). LC/MS (ESI, *m/z*) 329 [M−H_2−Cl]$^-$.

*4.1.1.8. (Z)-5′-(trifluoromethoxy)-[2,3′-biindolinylidene]-2′,3-dione **(1h)**.* 5-Trifluoromethoxyisatin (1000 mg, 4.33 mmol) and 3-acetoxyindole (758 mg, 4.33 mmol) were used and **1 h** (541 mg, 36 %, purple solid) was obtained. ^{1}H NMR (400 MHz, DMSO-d_6) δ 11.07 (d, J = 28.0 Hz, 2H), 8.74 (s, 1H), 7.64 (d, J = 8.0 Hz, 1H), 7.56 (t, J = 8.0 Hz, 1H), 7.40 (d, J = 8.0 Hz, 1H), 7.21 (d, J = 8.0 Hz, 1H), 7.01 (t, J = 7.0 Hz, 1H), 6.93 (d, J = 8.0 Hz, 1H). RP-HPLC (254 nm): 94 % (t_R = 16.6 min). LC/MS (ESI, *m/z*) 345 [M−H]$^-$.

4.1.2. General procedure for **2**–**8**

To solution of indirubin derivatives (**1**) in pyridine (0.15 M) was added the anhydrous hydroxylamine hydrochloride (7 eq) or O-alkylhydroxylamine (alkyl: methyl, ethyl, propyl, isopropyl, isobutyl, and benzyl) hydrochloride (7 eq). The reaction mixture was stirred and refluxed for overnight. After reacting, the solvent was evaporated under reduced pressure and the residue was diluted with water (added HCl cat.) and ethyl acetate in sonication for 1 h then extracted with ethyl acetate, and dried over anhydrous Na_2SO_4. The solvent was evaporated under reduced pressure and the residue was recrystallized from ethanol, and the red-brown precipitate was filtered and washed with hexane. Washed compound was dried under reduced pressure.

*4.1.2.1. (2Z,3E)-6′-bromo-3-(hydroxyimino)-[2,3′-biindolinylidene]-2′-one **(BIO)**.* **1a** (90 mg, 0.26 mmol) was used and **BIO** (32 mg, 34 %, red-brown solid) was obtained. mp 287–289 ℃. ^{1}H NMR (400 MHz, DMSO-d_6) δ 13.58 (s, 1H), 11.72 (s, 1H), 10.82 (s, 1H), 8.52 (d, J = 8.4 Hz, 1H), 8.19 (d, J = 7.6 Hz, 1H), 7.40–7.35 (m, 2H), 7.07–6.99 (m, 3H). ^{13}C NMR (100 MHz, DMSO-d_6) δ 171.10, 151.76, 146.40, 145.17, 140.06, 132.52, 128.34, 124.65, 123.10, 122.42, 122.22, 118.25, 116.86, 112.20, 111.91, 98.14. RP-HPLC (254 nm): 99 % (t_R = 9.6 min). LC/MS (ESI, *m/z*) 354 [M−H]$^-$. HRMS (ESI): *m/z* [M−H]$^-$ calcd. for

$C_{16}H_9BrN_3O_2^-$: 353.9884, found: 353.9861.

*4.1.2.2. (2Z,3E)-3-(hydroxyimino)-6′-methyl-[2,3′-biindolinylidene]-2′-one (**2a**).* **1b** (100 mg, 0.36 mmol) was used and **2a** (63.3 mg, 60 %, red-brown solid) was obtained. mp 249–251 ℃. ^{1}H NMR (400 MHz, DMSO-d_6) δ 13.36 (s, 1H), 11.59 (s, 1H), 10.63 (s, 1H), 8.49 (d, J = 8.0 Hz, 1H), 8.20 (d, J = 8.0 Hz, 1H), 7.37–7.34 (m, 2H), 7.00–6.94 (m, 1H), 6.74 (d, J = 8.0 Hz, 1H), 6.49 (s, 1H), 2.29 (s, 3H). ^{13}C NMR (100 MHz, DMSO-d_6) δ 171.6, 151.7, 145.3, 144.7, 139.1, 136.0, 132.4, 128.4, 123.4, 121.6, 121.5, 120.5, 116.9, 111.8, 110.0, 99.6, 21.8. RP-HPLC (254 nm): 98 % (t_R = 8.6 min). LC/MS (ESI, *m/z*) 292 $[M + H]^+$. HRMS (ESI): *m/z* $[M-H]^-$ calcd. for $C_{17}H_{12}N_3O_2^-$: 290.0935, found: 290.0938.

*4.1.2.3. (2Z,3E)-3-(hydroxyimino)-6′-(trifluoromethyl)-[2,3′-biindolinylidene]-2′-one (**2b**).* **1c** (200 mg, 0.64 mmol) was used and **2b** (60 mg, 29 %, red-brown solid) was obtained. mp 268–270 ℃. ^{1}H NMR (400 MHz, DMSO-d_6) δ 13.79 (s, 1H), 11.96 (s, 1H), 11.00 (s, 1H), 8.78 (d, J = 10.8 Hz, 1H), 8.24 (d, J = 10.0 Hz, 1H), 7.49–7.41 (m, 2H), 7.27–7.24 (m, 1H), 7.13–7.06 (m, 2H). ^{13}C NMR (100 MHz, DMSO-d_6) δ 171.15, 151.71, 147.99, 144.99, 138.51, 132.60, 128.32, 126.90, 125.70, 125.38, 122.92, 122.68, 117.30, 116.87, 112.50, 105.27, 97.49. RP-HPLC (254 nm): 99 % (t_R = 10.1 min). LC/MS (ESI, *m/z*) 344 $[M-H]^-$. HRMS (ESI): *m/z* $[M-H]^-$ calcd. for $C_{17}H_9F_3N_3O_2^-$: 344.0652, found: 344.0648.

*4.1.2.4. (2Z,3E)-3-(hydroxyimino)-6′-(trifluoromethoxy)-[2,3′-biindolinylidene]-2′-one (**2c**).* **1d** (100 mg, 0.26 mmol) was used and **2c** (89 mg, 92 %, red-brown solid) was obtained. mp 256–258 ℃. ^{1}H NMR (400 MHz, DMSO-d_6) δ 13.62 (s, 1H), 11.76 (s, 1H), 10.92 (s, 1H), 8.70 (d, J = 11.2 Hz, 1H), 8.24 (d, J = 10.0 Hz, 1H), 7.46–7.39 (m, 2H), 7.09–7.03 (m, 1H), 6.92–6.88 (m, 1H), 6.84–6.83 (m, 1H). ^{13}C NMR (100 MHz, DMSO-d_6) δ 171.41, 151.68, 146.57, 146.49, 146.48, 145.21, 139.70, 132.55, 128.34, 124.04, 122.37, 122.28, 116.88, 112.88, 112.27, 102.15, 97.81. RP-HPLC (254 nm): 97 % (t_R = 10.4 min). LC/MS (ESI, *m/z*) 360 $[M-H]^-$. HRMS (ESI): *m/z* $[M-H]^-$ calcd. for $C_{17}H_9F_3N_3O_3^-$: 360.0601, found: 360.0608.

*4.1.2.5. (2Z,3E)-5′-bromo-3-(hydroxyimino)-[2,3′-biindolinylidene]-2′-one (**2d**).* **1e** (250 mg, 0.84 mmol) was used and **2d** (35 mg, 13 %, red-brown solid) was obtained. mp 298–300 ℃. ^{1}H NMR (400 MHz, DMSO-d_6) δ 13.72 (s, 1H), 11.85 (s, 1H), 10.88 (s, 1H), 8.77 (d, J = 2.0 Hz, 1H), 8.25 (d, J = 7.6 Hz, 2H), 7.46–7.40 (m, 1H), 7.28 (dd, J = 8.4, 2.0 Hz, 1H), 7.08–7.04 (m, 1H), 6.85 (d, J = 8.0 Hz, 1H). ^{13}C NMR (100 MHz, DMSO-d_6) δ 171.06, 151.94, 146.86, 145.15, 137.64, 132.62, 128.49, 128.42, 125.25(2), 122.39, 116.95, 113.12, 112.30, 110.92, 98.12. RP-HPLC (254 nm): 95 % (t_R = 9.8 min). LC/MS (ESI, *m/z*) 354 $[M-H]^-$. HRMS (ESI): *m/z* $[M-H]^-$ calcd. for $C_{16}H_9BrN_3O_2^-$: 353.9884, found: 353.9875.

*4.1.2.6. (2Z,3E)-3-(hydroxyimino)-5′-methyl-[2,3′-biindolinylidene]-2′-one (**2e**).* **1f** (250 mg, 0.91 mmol) was used and **2e** (80 mg, 30 %, red-brown solid) was obtained. mp 275–277 ℃. ^{1}H NMR (400 MHz, DMSO-d_6) δ 13.37 (s, 1H), 11.70 (s, 1H), 10.57 (s, 1H), 8.46 (s, 1H), 8.21 (d, J = 8.0 Hz, 1H), 7.38–7.35 (m, 2H), 7.00–6.96 (m, 1H), 6.91 (d, J = 8.0 Hz, 1H), 6.75 (d, J = 4.0 Hz, 1H), 2.31 (s, 3H). ^{13}C NMR (100 MHz, DMSO-d_6) δ 171.5, 151.6, 145.4, 145.3, 136.5, 132.4, 129.3, 128.3, 126.8, 124.1, 123.1, 121.7, 116.9, 111.8, 108.8, 99.6, 21.8. RP-HPLC (254 nm): 91 % (t_R = 8.7 min). LC/MS (ESI, *m/z*) 292 $[M + H]^+$. HRMS (ESI): *m/z* $[M-H]^-$ calcd. for $C_{17}H_{12}N_3O_2^-$: 290.0935, found: 290.0947.

*4.1.2.7. (2Z,3E)-3-(hydroxyimino)-5′-(trifluoromethyl)-[2,3′-biindolinylidene]-2′-one hydrochloride (**2f**).* **1 g** (200 mg, 0.48 mmol) was used and **2f** (171 mg, 90 %, red-brown solid) was obtained. mp 315–317 ℃. ^{1}H NMR (400 MHz, DMSO-d_6) δ 13.64 (s, 1H), 12.44 (s, 1H), 11.82 (s, 1H), 11.07 (s, 1H), 9.17 (d, J = 2.4 Hz, 1H), 8.27 (d, J = 10.0 Hz, 1H), 7.80 (dd, J = 11.2, 2.4 Hz, 1H), 7.45–7.39 (m, 2H), 7.10–7.02 (m, 1H), 6.98 (dd, J = 14.8, 4.8 Hz, 1H). ^{13}C NMR (100 MHz, DMSO-d_6) δ 171.60, 168.52, 152.11, 146.66, 145.05, 142.14, 132.52, 128.59, 128.41, 124.55, 123.49, 122.95, 122.26, 117.06, 112.16, 108.83, 98.31. RP-HPLC (254 nm): 97 % (t_R = 6.0 min). LC/MS (ESI, *m/z*) 344 $[M-H_2-Cl]^-$. HRMS (ESI): *m/z* $[M-H_2-Cl]^-$ calcd. for $C_{17}H_9F_3N_3O_2^-$: 344.0652, found: 344.0653.

*4.1.2.8. (2Z,3E)-3-(hydroxyimino)-5′-(trifluoromethoxy)-[2,3′-biindolinylidene]-2′-one (**2g**).* **1 h** (250 mg, 0.72 mmol) was used and **2 g** (50 mg, 22 %, red-brown solid) was obtained. mp 292–294 ℃. ^{1}H NMR (400 MHz, DMSO-d_6) δ 13.63 (s, 1H), 11.82 (s, 1H), 10.87 (s, 1H), 8.58 (s, 1H), 8.21 (d, J = 8.0 Hz, 1H), 7.42–7.36 (m, 2H), 7.08–7.01 (m, 2H), 6.92 (d, J = 8.0 Hz, 1H). ^{13}C NMR (100 MHz, DMSO-d_6) δ 171.32, 151.84, 145.89, 145.50, 142.98, 137.86, 133.51, 128.78, 123.76, 122.41, 119.52, 116.53, 116.37, 112.60, 109.78, 99.70, 64.63. RP-HPLC (254 nm): 97 % (t_R = 10.6 min). LC/MS (ESI, *m/z*) 360 $[M-H]^-$. HRMS (ESI): *m/z* $[M-H]^-$ calcd. for $C_{17}H_9F_3N_3O_3^-$: 360.0601, found: 360.0578.

*4.1.2.9. (2Z,3E)-6′-bromo-3-(methoxyimino)-[2,3′-biindolinylidene]-2′-one (**3a**).* **1a** (200 mg, 0.59 mmol) was used and **3a** (162 mg, 73 %, red-brown solid) was obtained. mp 286–288 ℃. ^{1}H NMR (400 MHz, DMSO-d_6) δ 11.70 (s, 1H), 10.91 (s, 1H), 8.53 (d, J = 8.4 Hz, 1H), 8.10 (d, J = 7.6 Hz, 1H), 7.44 (d, J = 3.6 Hz, 2H), 7.17 (d, J = 8.4 Hz, 1H), 7.06–7.03 (m, 2H), 4.38 (s, 3H). ^{13}C NMR (100 MHz, DMSO-d_6) δ 171.07, 151.62, 145.90, 145.00, 140.47, 133.39, 128.71, 125.18, 123.60, 122.22, 122.09, 118.76, 116.56, 112.48, 112.00, 99.50, 64.92. EA: C: 55.19, H: 3.27, N: 11.36. RP-HPLC (254 nm): 98 % (t_R = 14.8 min). LC/MS (ESI, *m/z*) 370 $[M + H]^+$.

*4.1.2.10. (2Z,3E)-5′-bromo-3-(methoxyimino)-[2,3′-biindolinylidene]-2′-one (**3b**).* **1e** (200 mg, 0.57 mmol) was used and **3b** (31 mg, 14 %, red-brown solid) was obtained. mp 301–303 ℃. ^{1}H NMR (400 MHz, DMSO-d_6) δ 11.66 (s, 1H), 10.84 (s, 1H), 8.80 (s, 1H), 8.05 (d, J = 8.0 Hz, 1H), 7.42–7.37 (m, 2H), 7.24 (d, J = 8.0 Hz, 1H), 7.03–6.96 (m, 1H), 6.80 (d, J = 8.0 Hz, 1H), 4.34 (s, 3H). ^{13}C NMR (100 MHz, DMSO-d_6) δ 170.93, 151.65, 145.93, 145.36, 138.06, 133.50, 128.75, 128.71, 125.99, 124.89, 122.37, 116.49, 112.94, 112.61, 111.03, 99.37, 64.88. RP-HPLC (254 nm): 92 % (t_R = 15.0 min). LC/MS (ESI, *m/z*) 370 $[M + H]^+$. HRMS (ESI): *m/z* $[M + H]^-$ calcd. for $C_{17}H_{13}BrN_3O_2^-$: 370.0186, found: 370.0023.

*4.1.2.11. (2Z,3E)-3-(methoxyimino)-5′-(trifluoromethyl)-[2,3′-biindolinylidene]-2′-one hydrochloride (**3c**).* **1 g** (100 mg, 0.27 mmol) was used and **3c** (90 mg, 82 %, red-brown solid) was obtained. mp 284–286 ℃. ^{1}H NMR (400 MHz, DMSO-d_6) δ 12.45 (s, 1H), 11.65 (s, 1H), 11.09 (s, 1H), 9.43 (d, J = 1.2 Hz, 1H), 8.12 (d, J = 7.6 Hz, 1H), 7.81 (dd, J = 8.4, 1.6 Hz, 1H), 7.45 (d, J = 4.0 Hz, 2H), 7.09–7.03 (m, 1H), 6.98 (d, J = 8.0 Hz, 1H), 4.46 (s, 3H). ^{13}C NMR (100 MHz, DMSO-d_6) δ 171.52, 168.41, 151.37, 145.94, 145.19, 142.61, 133.32, 128.74, 128.53, 125.61, 123.46, 122.59, 122.20, 116.49, 112.50, 108.95, 99.63, 65.02. RP-HPLC (254 nm): 98 % (t_R = 7.2 min). LC/MS (ESI, *m/z*) 360 $[M-Cl]^+$. HRMS (ESI): *m/z* $[M-H_2-Cl]^-$ calcd. for $C_{18}H_{11}F_3N3O_2^-$: 358.0809, found: 358.0807.

*4.1.2.12. (2Z,3E)-6′-bromo-3-(ethoxyimino)-[2,3′-biindolinylidene]-2′-one (**4a**).* **1a** (100 mg, 0.30 mmol) was used and **4a** (80 mg, 71 %, red-brown solid) was obtained. mp 319–321 ℃. ^{1}H NMR (400 MHz, DMSO-d_6) δ 11.71 (s, 1H), 10.91 (s, 1H), 8.55 (d, J = 8.4 Hz, 1H), 8.13 (d, J = 7.6 Hz, 1H), 7.45 (d, J = 4.0 Hz, 2H), 7.17 (d, J = 8.4 Hz, 1H), 7.07–7.04 (m, 2H), 4.66 (q, J = 7.2 Hz, 2H), 1.51 (t, J = 7.2 Hz, 3H). EA: C: 56.14, H: 3.77, N: 10.90. RP-HPLC (254 nm): 99 % (t_R = 16.1 min). LC/MS (ESI, *m/z*) 384 $[M + H]^+$. HRMS (ESI): *m/z* $[M + H]^-$ calcd. for

$C_{18}H_{15}BrN_3O_2^-$: 384.0342, found: 384.0187.

*4.1.2.13. (2Z,3E)-5′-bromo-3-(ethoxyimino)-[2,3′-biindolinylidene]-2′-one (**4b**).* **1e** (300 mg, 0.88 mmol) was used and **4b** (90 mg, 26 %, red-brown solid) was obtained. mp 273–275 ℃. ^{1}H NMR (400 MHz, DMSO-d_6) δ 11.68 (s, 1H), 10.84 (s, 1H), 8.81 (s, 1H), 8.07 (d, J = 8.0 Hz, 1H), 7.42–7.37 (m, 2H), 7.25–7.23 (m, 1H), 7.03–6.99 (m, 1H), 6.80 (d, J = 8.0 Hz, 1H), 4.60 (q, J = 8.0 Hz, 2H), 1.51 (t, J = 8.0 Hz, 3H). ^{13}C NMR (100 MHz, DMSO-d_6) δ 170.8, 151.4, 145.7, 145.4, 137.9, 133.2, 128.5, 128.5, 125.6, 124.8, 122.2, 116.4, 112.9, 112.4, 110.9, 99.1, 72.6, 14.9. RP-HPLC (254 nm): 98 % (t_R = 16.2 min). LC/MS (ESI, m/z) 384 $[M + H]^+$. HRMS (ESI): m/z $[M + H]^-$ calcd. for $C_{18}H_{15}BrN_3O_2^-$: 384.0342, found: 384.0176.

*4.1.2.14. (2Z,3E)-3-(ethoxyimino)-5′-(trifluoromethyl)-[2,3′-biindolinylidene]-2′-one hydrochloride (**4c**).* **1 g** (100 mg, 0.27 mmol) was used and **4c** (90 mg, 81 %, red-brown solid) was obtained. mp 317–319 ℃. ^{1}H NMR (400 MHz, DMSO-d_6) δ 12.43 (s, 1H), 11.68 (s, 1H), 11.09 (s, 1H), 9.41 (s, 1H), 8.14 (d, J = 7.6 Hz, 1H), 7.80 (d, J = 8.4 Hz, 1H), 7.45 (d, J = 4.0 Hz, 2H), 7.08–7.04 (m, 1H), 6.98 (d, J = 8.4 Hz, 1H), 4.74 (q, J = 7.2 Hz, 2H), 1.52 (t, J = 7.0 Hz, 3H). ^{13}C NMR (100 MHz, DMSO-d_6) δ 171.56, 168.41, 151.30, 145.83, 145.37, 142.53, 133.22, 128.63, 128.51, 125.44, 123.48, 122.67, 122.21, 116.57, 112.45, 108.94, 99.41, 72.95, 15.19. RP-HPLC (254 nm): 95 % (t_R = 8.2 min). LC/MS (ESI, m/z) 374 $[M-Cl]^+$. HRMS (ESI): m/z $[M-H_2-Cl]^-$ calcd. for $C_{19}H_{13}F_3N_3O_2^-$: 372.0965, found: 372.0957.

*4.1.2.15. (2Z,3E)-6′-bromo-3-(propoxyimino)-[2,3′-biindolinylidene]-2′-one (**5a**).* **1a** (50 mg, 0.15 mmol) was used and **5a** (28 mg, 46 %, red-brown solid) was obtained. mp 298–300 ℃. ^{1}H NMR (400 MHz, DMSO-d_6) δ 11.71 (s, 1H), 10.91 (s, 1H), 8.54 (d, J = 8.4 Hz, 1H), 8.12 (d, J = 7.2 Hz, 1H), 7.45 (d, J = 3.6 Hz, 2H), 7.17 (d, J = 8.4 Hz, 1H), 7.08–7.04 (m, 2H), 4.58 (t, J = 6.4 Hz, 2H), 1.94–1.89 (m, 2H), 1.05 (t, J = 7.2 Hz, 3H). EA: C: 57.34, H: 4.13, N: 10.43. RP-HPLC (254 nm): 96 % (t_R = 17.8 min). LC/MS (ESI, m/z) 398 $[M + H]^+$. HRMS (ESI): m/z $[M + H]^-$ calcd. for $C_{19}H_{17}BrN_3O_2^-$: 398.0499, found: 398.0346.

*4.1.2.16. (2Z,3E)-5′-bromo-3-(propoxyimino)-[2,3′-biindolinylidene]-2′-one (**5b**).* **1e** (300 mg, 0.88 mmol) was used and **5b** (97 mg, 28 %, red-brown solid) was obtained. mp 246–248 ℃. ^{1}H NMR (400 MHz, DMSO-d_6) δ 11.75 (s, 1H), 10.92 (s, 1H), 8.88 (d, J = 2.0 Hz, 1H), 8.13 (d, J = 7.6 Hz, 1H), 7.46 (d, J = 4.0 Hz, 2H), 7.30 (dd, J = 8.4, 2.4 Hz, 1H), 7.11–7.05 (m, 1H), 6.86 (d, J = 8.0 Hz, 1H), 4.57 (t, J = 6.8 Hz, 2H), 2.03–1.94 (m, 2H), 1.07 (t, J = 7.4 Hz, 3H). ^{13}C NMR (100 MHz, DMSO-d_6) δ 170.95, 151.57, 145.82, 145.50, 137.99, 133.37, 128.59, 128.54, 125.75, 124.95, 122.38, 116.55, 112.93, 112.56, 110.99, 99.19, 78.52, 22.59, 10.66. RP-HPLC (254 nm): 98 % (t_R = 17.9 min). LC/MS (ESI, m/z) 398 $[M + H]^+$. HRMS (ESI): m/z $[M + H]^-$ calcd. for $C_{19}H_{17}BrN_3O_2^-$: 398.0499, found: 398.0341.

*4.1.2.17. (2Z,3E)-3-(propoxyimino)-5′-(trifluoromethyl)-[2,3′-biindolinylidene]-2′-one hydrochloride (**5c**).* **1 g** (70 mg, 0.19 mmol) was used and **5c** (61 mg, 75 %, red-brown solid) was obtained. mp 313–315 ℃. ^{1}H NMR (400 MHz, DMSO-d_6) δ 12.47 (s, 1H), 11.68 (s, 1H), 11.09 (s, 1H), 9.41 (d, J = 1.2 Hz, 1H), 8.14 (d, J = 7.6 Hz, 1H), 7.80 (dd, J = 8.0, 1.6 Hz, 1H), 7.46 (d, J = 4.0 Hz, 2H), 7.10–7.04 (m, 1H), 6.98 (d, J = 8.0 Hz, 1H), 4.66 (t, J = 6.8 Hz, 2H), 1.99–1.89 (m, 2H), 1.04 (t, J = 7.4 Hz, 3H). ^{13}C NMR (100 MHz, DMSO-d_6) δ 171.55, 168.46, 151.28, 145.82, 145.37, 142.53, 133.21, 128.65, 128.40, 125.45, 123.48, 122.66, 122.25, 116.58, 112.48, 108.94, 99.40, 78.77, 22.77, 10.53. RP-HPLC (254 nm): 90 % (t_R = 9.5 min). LC/MS (ESI, m/z) 388 $[M-Cl]^+$. HRMS (ESI): m/z $[M-H_2-Cl]^-$ calcd. for $C_{20}H_{15}F_3N_3O_2^-$: 386.1122, found: 386.1119.

*4.1.2.18. (2Z,3E)-6′-bromo-3-(isopropoxyimino)-[2,3′-biindolinylidene]-2′-one (**6a**).* **1a** (80 mg, 0.23 mmol) was used and **6a** (63 mg, 67 %, red-brown solid) was obtained. mp 304–306 ℃. ^{1}H NMR (400 MHz, DMSO-d_6) δ 11.72 (s, 1H), 10.91 (s, 1H), 8.57 (d, J = 8.0 Hz, 1H), 8.13 (d, J = 7.6 Hz, 1H), 7.44 (d, J = 3.6 Hz, 2H), 7.16 (d, J = 8.4 Hz, 1H), 7.08–7.04 (m, 2H), 4.91–4.86 (m, 1H), 1.50 (d, J = 6.0 Hz, 6H). EA: C: 57.33, H: 4.16, N: 10.66. RP-HPLC (254 nm): 98 % (t_R = 17.4 min). LC/MS (ESI, m/z) 398 $[M + H]^+$. HRMS (ESI): m/z $[M + H]^-$ calcd. for $C_{19}H_{17}BrN_3O_2^-$: 398.0499, found: 398.0327.

*4.1.2.19. (2Z,3E)-5′-bromo-3-(isopropoxyimino)-[2,3′-biindolinylidene]-2′-one (**6b**).* **1e** (70 mg, 0.20 mmol) was used and **6b** (44 mg, 54 %, red-brown solid) was obtained. mp 311−313℃. ^{1}H NMR (400 MHz, DMSO-d_6) δ 11.75 (s, 1H), 10.89 (s, 1H), 8.90 (d, J = 2.0 Hz, 1H), 8.13 (d, J = 7.6 Hz, 1H), 7.45 (d, J = 4.0 Hz, 2H), 7.30 (dd, J = 8.0, 2.0 Hz, 1H), 7.10–7.04 (m, 1H), 6.86 (d, J = 8.4 Hz, 1H), 4.91–4.81 (m, 1H), 1.56 (d, J = 6.4 Hz, 6H). ^{13}C NMR (100 MHz, DMSO-d_6) δ 170.98, 151.41, 145.76, 145.63, 137.93, 133.32, 128.65, 128.55, 125.54, 125.02, 122.38, 116.62, 112.96, 112.52, 111.03, 99.03, 79.29, 21.80 (2). RP-HPLC (254 nm): 97 % (t_R = 17.6 min). LC/MS (ESI, m/z) 398 $[M + H]^+$. HRMS (ESI): m/z $[M + H]^-$ calcd. for $C_{19}H_{17}BrN_3O_2^-$: 398.0499, found: 398.0358.

*4.1.2.20. (2Z,3E)-3-(isopropoxyimino)-5′-(trifluoromethyl)-[2,3′-biindolinylidene]-2′-one hydrochloride (**6c**).* **1 g** (70 mg, 0.19 mmol) was used and **6c** (66 mg, 79 %, red-brown solid) was obtained. mp 321–323 ℃. ^{1}H NMR (400 MHz, DMSO-d_6) δ 12.42 (s, 1H), 11.72 (s, 1H), 11.09 (s, 1H), 9.40 (d, J = 1.2 Hz, 1H), 8.15 (d, J = 7.6 Hz, 1H), 7.80 (dd, J = 8.4, 1.6 Hz, 1H), 7.45 (d, J = 4.0 Hz, 2H), 7.09–7.05 (m, 1H), 6.98 (d, J = 8.0 Hz, 1H), 5.05–4.95 (m, 1H), 1.53 (d, J = 6.0 Hz, 6H). ^{13}C NMR (100 MHz, DMSO-d_6) δ 171.57, 168.42, 151.09, 145.75, 145.48, 142.45, 133.17, 128.57, 128.54, 125.29, 123.51, 122.72, 122.24, 116.62, 112.46, 108.95, 99.19, 79.59, 21.97(2). RP-HPLC (254 nm): 95 % (t_R = 9.3 min). LC/MS (ESI, m/z) 388 $[M-Cl]^+$. HRMS (ESI): m/z $[M + H]^+$ calcd. for $C_{20}H_{16}F_3N_3O_2^-$: 388.1267, found: 388.1282.

*4.1.2.21. (2Z,3E)-6′-bromo-3-(isobutoxyimino)-[2,3′-biindolinylidene]-2′-one (**7a**).* **1a** (50 mg, 0.15 mmol) was used and **7a** (12 mg, 20 %, red-brown solid) was obtained. mp 280–282 ℃. ^{1}H NMR (400 MHz, DMSO-d_6) δ 11.71 (s, 1H), 10.91 (s, 1H), 8.54 (d, J = 8.4 Hz, 1H), 8.11 (d, J = 7.2 Hz, 1H), 7.45 (d, J = 4.0 Hz, 2H), 7.18 (d, J = 8.4 Hz, 1H), 7.06–7.03 (m, 2H), 4.42 (d, J = 6.4 Hz, 2H), 2.26–2.19 (m, 1H), 1.06 (d, J = 6.4 Hz, 6H). EA: C: 58.34, H: 4.32, N: 10.33. RP-HPLC (254 nm): 98 % (t_R = 19.2 min). LC/MS (ESI, m/z) 412 $[M + H]^+$. HRMS (ESI): m/z $[M-H]^-$ calcd. for $C_{20}H_{17}BrN_3O_2^-$: 410.0510, found: 410.0507.

*4.1.2.22. (2Z,3E)-5′-bromo-3-(isobutoxyimino)-[2,3′-biindolinylidene]-2′-one (**7b**).* **1e** (70 mg, 0.20 mmol) was used and **7b** (74 mg, 92 %, red-brown solid) was obtained. mp 269–271 ℃. ^{1}H NMR (400 MHz, DMSO-d_6) δ 11.74 (s, 1H), 10.89 (s, 1H), 8.87 (s, 1H), 8.12 (d, J = 7.6 Hz, 1H), 7.46 (d, J = 4.0 Hz, 2H), 7.30 (d, J = 8.4 Hz, 1H), 7.10–7.07 (m, 1H), 6.86 (dd, J = 8.0, 0.8 Hz, 1H), 4.41 (d, J = 6.0 Hz, 2H), 2.38–2.30 (m, 1H), 1.07 (t, J = 3.2 Hz, 6H). ^{13}C NMR (100 MHz, DMSO-d_6) δ 170.91, 151.51, 145.82, 145.47, 137.97, 133.38, 128.59, 128.41, 125.74, 124.92, 122.41, 116.52, 112.90, 112.59, 110.99, 99.18, 83.30, 28.43, 19.29(2). RP-HPLC (254 nm): 91 % (t_R = 19.8 min). LC/MS (ESI, m/z) 412 $[M + H]^+$. HRMS (ESI): m/z $[M-H]^-$ calcd. for $C_{20}H_{17}BrN_3O_2^-$: 410.0510, found: 410.0491.

*4.1.2.23. (2Z,3E)-3-(isobutoxyimino)-5′-(trifluoromethyl)-[2,3′-biindolinylidene]-2′-one hydrochloride (**7c**).* **1 g** (60 mg, 0.16 mmol) was used and **7c** (63 mg, 80 %, red-brown solid) was obtained. mp 308–310 ℃. ^{1}H NMR (400 MHz, DMSO-d_6) δ 12.50 (s, 1H), 11.69 (s, 1H), 11.09 (s, 1H), 9.42 (d, J = 1.2 Hz, 1H), 8.13 (d, J = 8.0 Hz, 1H), 7.80 (dd, J = 8.4, 1.6 Hz, 1H), 7.46 (d, J = 3.2 Hz, 2H), 7.12–7.05 (m, 1H), 6.98 (d, J = 8.0 Hz,

1H). 4.52 (d, $J = 6.8$ Hz, 2H), 2.31–2.24 (m, 1H), 1.04 (d, $J = 6.8$ Hz, 6H). ^{13}C NMR (100 MHz, DMSO-d_6) δ 171.55, 168.51, 151.21, 145.83, 145.38, 142.54, 133.23, 128.67, 128.28, 125.48, 123.47, 122.66, 122.30, 116.59, 112.52, 108.94, 99.40, 83.52, 28.55, 19.22(2). RP-HPLC (254 nm): 91 % (t_R = 10.7 min). LC/MS (ESI, *m/z*) 402 $[M-Cl]^+$. $[M + H]^+$ calcd. for $C_{21}H_{18}F_3N_3O_2^-$: 402.1424, found: 402.1445.

*4.1.2.24. (2Z,3E)-3-((benzyloxy)imino)-6′-bromo-[2,3′-biindolinylidene]-2′-one (**8a**).* **1a** (80 mg, 0.23 mmol) was used and **8a** (73 mg, 56 %, red-brown solid) was obtained. mp 277–279 ℃. ^{1}H NMR (400 MHz, DMSO-d_6) δ 11.66 (s, 1H), 10.88 (s, 1H), 8.31 (d, $J = 8.4$ Hz, 1H), 8.17 (d, $J = 7.6$ Hz, 1H), 7.59 (d, $J = 7.6$ Hz, 2H), 7.47–7.37 (m, 5H), 7.05–6.99 (m, 3H), 5.63 (s, 2H). EA: C: 61.93, H: 3.64, N: 9.40. RP-HPLC (254 nm): 99 % ($t_R = 16.8$ min). LC/MS (ESI, *m/z*) 446 $[M + H]^+$. HRMS (ESI): *m/z* $[M + H]^-$ calcd. for $C_{23}H_{17}BrN_3O_2^-$: 446.0499, found: 446.0336. $[M + H]^+$ calcd. for $C_{20}H_{16}F_3N_3O_2^-$: 388.1267, found: 388.1282.

*4.1.2.25. (2Z,3E)-3-((benzyloxy)imino)-5′-bromo-[2,3′-biindolinylidene]-2′-one (**8b**).* **1e** (150 mg, 0.44 mmol) was used and **8b** (35 mg, 18 %, red-brown solid) was obtained. mp 302–304 ℃. ^{1}H NMR (400 MHz, DMSO-d_6) δ 11.61 (s, 1H), 10.84 (s, 1H), 8.33 (d, $J = 8.0$ Hz, 1H), 8.14 (d, $J = 8.0$ Hz, 1H), 7.55 (d, $J = 8.0$ Hz, 2H), 7.46–7.29 (m, 5H), 7.06–6.97 (m, 1H), 6.90–6.80 (m, 2H), 5.60 (s, 2H). EA: C, 61.01; H, 3.39; N, 10.17. RP-HPLC (254 nm): 99 % ($t_R = 17.3$ min). LC/MS (ESI, *m/z*) 446 $[M + H]^+$. HRMS (ESI): *m/z* $[M-H]^-$ calcd. for $C_{23}H_{15}BrN_3O_2^-$: 444.0353, found: 444.0326.

*4.1.2.26. (2Z,3E)-3-((benzyloxy)imino)-5′-(trifluoromethyl)-[2,3′-biindolinylidene]-2′-one hydrochloride (**8c**).* **1 g** (70 mg, 0.19 mmol) was used and **8c** (75 mg, 78 %, red-brown solid) was obtained. mp 317–319 ℃. ^{1}H NMR (400 MHz, DMSO-d_6) δ 12.55 (s, 1H), 11.66 (s, 1H), 11.11 (s, 1H), 9.52 (s, 1H), 8.14 (d, $J = 7.6$ Hz, 1H), 7.83 (d, $J = 8.0$ Hz, 1H), 7.62 (d, $J = 8.0$ Hz, 2H), 7.45–7.34 (m, 5H), 7.07–7.04 (m, 1H), 6.99 (d, $J = 8.0$ Hz, 1H), 5.78 (s, 2H). ^{13}C NMR (100 MHz, DMSO-d_6) δ ^{13}C NMR (100 MHz, DMSO-d_6) δ 171.51, 168.49, 151.88, 145.97, 145.14, 142.64, 137.31, 133.42, 129.05(2), 128.92(2), 128.88, 128.83, 128.54, 125.57, 123.47, 122.60, 122.30, 116.57, 112.54, 109.01, 99.72, 79.04. RP-HPLC (254 nm): 94 % ($t_R = 10.1$ min). LC/MS (ESI, *m/z*) 434 $[M-H_2-Cl]^-$. $[M + H]^+$ calcd. for $C_{24}H_{16}F_3N_3O_2^-$: 436.1267, found: 436.1284.

4.2. Inhibition of GSK-3β

All compounds were prepared to 50x final assay concentration in 100 % DMSO. This working stock of the compound was added to the assay well as the first component in the reaction. GSK-3β (human) was incubated with 8 mM MOPS pH 7.0, 0.2 mM EDTA, 20 μM YRRAAVPPSPSLSRHSSPHQS(p) EDEEE (phospho GS2 peptide), 10 mM Magnesium acetate and [8-33P]-ATP (specific activity and concentration as required). Kinases are diluted in the buffer (20 mM MOPS, 1 mM EDTA, 0.01 % Brij-35, 5 % Glycerol, 0.1 % 5-mercaptoethanol, and 1 mg/mL BSA) shown below prior to addition to the reaction mix. The reaction was initiated by the addition of the Mg/ATP mix. This assay was conducted at a concentration within 15 μM of the apparent K_M for ATP. After incubation for 40 min at room temperature, the reaction was stopped by the addition of phosphoric acid to a concentration of 0.5 %. 10 μL of the reaction was then spotted onto a P30 filtermat and washed four times for 4 min in 0.425 % phosphoric acid and once in methanol prior to drying and scintillation counting. Positive control (Staurosporin) wells contained all components of the reaction. DMSO (at a final concentration of 2 %) was included in these wells to control for solvent effects. Blank wells contained all components of the reaction, with a reference inhibitor replacing the compound of interest. This abolished kinase activity and established the base-line (0 % kinase activity remaining). The blank wells were generated by omitting the enzyme. These experiments were performed at Eurofins Cerep SA (Celle L'Evescault, France).

4.3. Inhibition of CXXC5-Dvl interaction

100 μL of 5 mg/ml purified Dvl PDZ domain was added into each well of a 96-well Black Immunoplate (SPL, Seoul, Korea) and incubated overnight in a 4 °C chamber. After washing with PBS, 100 μL of 10 μM PolyR-DBM [10] was added to each well and incubated for 4 h. After washing three times with binding buffer (1 mM ethylenediaminetetraacetic acid (EDTA) and 2 mM dithiothreitol (DTT) in PBS), 1 μL of small molecule compound was treated with 100 μL of PBS in each well and incubated for 2 – 3 h at room temperature. After washing with binding buffer, the fluorescence in each well was measured using a Fluorstar Optima microplate reader (BGM Lab Technologie, Ortenberg, Germany).

4.4. Wnt signaling

HEK293-TOP cells were seeded into 24-well plates at a density of 1×10^5 cells per well. The cells were treated with the indicated concentrations of each compound and incubated for 24 h. The cells were then harvested using ice-cold phosphate-buffered saline (PBS) and lysed in 100 μL of Reporter Lysis Buffer (Promega, Madison, US) according to the manufacturer's instructions. After centrifugation, the luciferase activity was measured using 35 μL of the supernatant. The relative luciferase activity was normalized to that of the DMSO-treated control. HEK293-TOP cells (HEK293 cells containing the chromosomally incorporated TOPFlash gene) were provided by Dr. S Oh (Kook Min University, Korea).

4.5. Western blotting assays

Cells were lysed in ice-cold RIPA lysis buffer consisting of 50 mM Tris-HCl (pH 7.5), 150 mM NaCl, 2 mM EDTA, 1 % Triton X-100, 0.1 % SDS, 0.5 % Sodium deoxycholate, and Complete™ EDTA-free Protease Inhibitor Cocktail (Roche Diagnostics, Indianapolis, IN, USA). Protein samples (15 – 30 μg) were electrophoresed in 10 % SDS–polyacrylamide gels and then transferred to nitrocellulose membranes (Amersham Pharmacia Biotech, Amersham, UK). After blocking with 5 % non-fat dried milk for 1 h, membranes were incubated with mouse anti-β-catenin (1:1000 dilution; #610154; BD Bioscience, Cowey, UK) and mouse anti-α-Tubulin (1:3000 dilution; #3873; (Cell Signalling Technology, Beverly, MA, USA) primary antibodies, followed by an HRP-conjugated secondary antibody (1:2000; Jackson ImmunoResearch, West Grove, PA, USA). Specific bands were detected by enhanced chemiluminescence (Thermo Fisher Scientific, Rockford, IL, USA).

4.6. Cell cytotoxicity assay

TOPflash HEK-293 cells were seeded at a density of 2.5×10^4 cells in each well of 96-well plates and treated with the indicated concentrations of each compound for 24 h. The cells were then incubated with MTT (3-(4,5-dimethylthiazol-2-yl)-2,5-diphenyltetrazolium bromide; Sigma-Aldrich, St Louis, MO, USA) solution at 37 °C for 2 h. Dark brown formazan crystals formed after the reduction of tetrazolium by the mitochondria of living cells dissolved in DMSO, and the optical densities of samples were read at 570 nm with a FLUOstar Optima microplate reader (BGM Lab Technologie, Ortenberg, Germany). The assay was carried out in triplicate.

4.7. Docking study

All the molecular docking analysis took Discovery Studio 2020 software (Biovia) adopting the CHARMm force field. X-ray crystal or

NMR structures of GSK-3β and Dvl protein (Protein Data Bank code 1UV5, 6LCB, and 2KAW) was obtained from the RCSB protein databank and was refined to remove water molecules and add hydrogen atoms to the entire enzyme. To dock the ligands, Ligandfit (PDB ID: 1UV5 and 6LCB) and CDOCKER (PDB ID: 2KAW) docking method was performed. The crystallographic ligand BIO (6-Bromoindirubin-3′-oxime, PDB ID: BRW), NPL3009 (2-[[3-[(2E)-2-[1,3-bis(oxidanylidene)-1-phenylbutan-2-ylidene]hydrazinyl]phenyl]sulfonylamino]benzoic acid, PDB ID: E83), and sulindac (PDB ID: SUZ [30]) were used to determine the binding site of 1UV5 and 2KAW, respectively. Compounds were docked to the binding site of proteins and 30 poses were generated for each. Based on the docking results, binding energy the most predictive binding mode were calculated. To compare the sequences and 3D-stuructures (PDB ID: 2KAW and 6LCB), Superimpose proteins were performed by sequence alignment, C-alpha pairs, and tethers

4.8. Microsomal stability

4.8.1. Method 1

Microsomal incubations were conducted in triplicate in 0.1 M potassium phosphate buffer (pH 7.4) in eight-well tube strips. To study NADPH-dependent metabolic stability, test compounds (1 mm) were incubated with pooled human liver microsomes at a final concentration of 0.5 $mgmL^{-1}$ (Corning, NY, USA), in the presence of NADPH in a final volume of 160 mL. Verapamil was used as a reference. The test compounds and microsomes were pre-incubated at 37 °C for 5 min, and the reaction was initiated by adding NADPH. The reaction was terminated at 0 min and 30 min by the addition of 160 mL of ice-cold chlopropamide and CH_3CN. The values for % remaining were analyzed by a liquid chromatography mass spectrometry (LC-MS/MS, Nexera XR system (Shimadzu) and TSQ vantage (Thermo)) for quantitation of compounds. These experiments were performed at the DGMIF new drug development center (Daegu, Korea).

4.8.2. Method 2

Liver S9 incubations were conducted in 50 mM Tris buffer (pH 7.4) in cluster tubes (n = 3). Test substance was dissolved in methanol to a concentration of 10 mM and diluted to a concentration of 120 μM using 50 % aqueous ethanol. 5 μL of test substance was mixed with a solution containing 10 μL of liver S9 fractions, 40 μL of 1 M Tris buffer (pH 7.4) containing 10 mM $MgCl_2$ and 125 μg/mL alamethicin and 125 μL of de-ionized water. The final incubation mixture contained 200 mM Tris-HCl (pH 7.4), 1 mg protein/mL liver S9 fractions, 3 μM test substance, 25 μg/mL alamethicin, 8 mM $MgCl_2$. The reaction was initiated by adding 20 μL of 10 mM NADPH, 5 mM UDPGA, 1 mM PAPS and 25 mM GSH mixture dissolved in de-ionized water and the final concentration of cofactors in the mixture were 1 mM NADPH, 0.5 mM UDPGA, 0.1 mM PAPS and 2.5 mM GSH, respectively. The reaction was terminated at selected times (0 and 60 min) by the addition of 200 μL ice-cold acetonitrile containing diclofenac (500 ng/mL) as the internal standard for sample analysis. All samples were vortexed, sonicated, and centrifuged at 3000 xg for 20 min and the supernatant was analyzed by Agilent 6530 Q-TOF LC-MS/MS system in a positive auto MS/MS scan mode.

4.9. Plasma stability

4.9.1. Method 1

To study plasma stability, test compounds (10 μM) were incubated with pooled human plasma (Sigma–Aldrich, MO, USA). Procaine and Enalapril were used as negative and positive controls. The test compounds and plasma were pre-incubated at 37 °C for 0, 30, and 120 min. The reaction was terminated at 0, 30, and 120 min by the addition of 160 mL of ice-cold chlopropamide and CH_3CN. The values for % remaining were analyzed by a liquid chromatography mass spectrometry (LC-MS/MS, Nexera XR system (Shimadzu) and TSQ vantage (Thermo)) for quantitation of compounds. These experiments were performed at the DGMIF new drug development center (Daegu, Korea).

4.9.2. Method 2

Human (IPLANAH) plasma was purchased from Innovative Research (Novi, Michigan, US). The Plasma samples were diluted 2-fold with 0.1 M phosphate buffer (pH 7.4). Test substance was dissolved in DMSO to a concentration of 10 mM and diluted to a concentration of 120 μM using water. 5 μL of test substance solution was added to plasma to a final volume of 200 μL and a final concentration of test substance was 3 μM. The reaction was terminated at selected times (0 and 60 min) by the addition of 200 μL ice-cold acetonitrile containing diclofenac (500 ng/mL) as the internal standard for sample analysis All samples were vortexed, sonicated, and centrifuged at 3000 xg for 30 min and the supernatant was analyzed by Agilent 6530 Q-TOF LC-MS/MS system in a positive auto MS/MS scan mode.

4.10. In vitro migration assay for wound healing

HaCaT cells, a human keratinocyte cell line, were cultured in Dulbecco's modified Eagle's medium (DMEM, Gibco, USA) supplemented with 10 % fetal bovine serum (FBS, Gibco) and 1 % penicillin/streptomycin (Gibco). The cells were seeded into 12-well plates at a density of 4 × 105 cells per well and incubated for 24 h at 37 ℃ in a humidified atmosphere containing 5 % CO_2. After incubation for 24 h, the cells were scratched in the middle of the cells using a 1000p tip. The scratched cells were treated with indirubin or indirubin derivates at a concentration of 1 μM. The cells treated with 0.1 % dimethyl sulfoxide (DMSO, Sigma, USA) were used as a negative control. The migrated cells were stained with 0.1 % crystal violet solution (Sigma, USA) at 24 h after treatment, and the relative wound healing rate was determined by wound area measured using Image J program.

4.11. Immunofluorescence staining

HaCaT cells were seeded at a density of 1×10^5 cells on coverslips in 24-well plates and treated with 1 μM indirubin or indirubin derivates for 24 hrs. Cells were fixed with 4 % (w/v) paraformaldehyde in phosphate-buffered saline (PBS) for 20 min and then washed three times with 0.1 % (w/v) BSA in PBS at room temperature. After blocking with 5 % BSA in PBS containing 0.3 % (v/v) Triton X-100 for 1 h at room temperature, cells were immunostained with rabbit polyclonal anti-β-Catenin primary antibody (#ab16051, 1:500 dilution, Abcam, Cambridge, UK) at 4 °C overnight. Subsequently, cells were washed three times with PBS and then labeled with 1:500 dilution of Alexa Fluor® 594-conjugated donkey anti-rabbit IgG (H + L) secondary antibody (#A-21207, Sigma-Aldrich, St Louis, MO, USA) for 1 h, before mounting with Vectashield mounting medium (Vector Laboratories, Burlingame, CA, USA) containing 4,6-diamidino-2-phenylindole (DAPI). Immunoreactive cells were detected and photographed using an epifluorescence microscope (Nikon Instruments, Melville, NY, USA) at magnifications ranging from 20 × to 40 × .

4.12. Statistical analyses

All quantitative data are expressed as means ± standard error of the mean (SEM). In each experiment, all measurements were performed at least in triplicate. Data were analyzed using a two-tailed, unpaired Student's *t*-test and values of $P < 0.05$ were considered statistically significant.

Declaration of Competing Interest

The authors declare that they have no known competing financial interests or personal relationships that could have appeared to influence the work reported in this paper.

Acknowledgement

This research was supported by a grant from the Translational Research Center for Protein Function Control (Grant NRF-2009-0083522), the Ministry of Science, the Ministry of Science and ICT (NRF-2019M3A9A8065095), the Bio & Medical Technology Development Program of the National Research Foundation (NRF) & funded by the Korean government (MSIP&MOHW) (Grant NRF-2016M3A9B5941215), the Korea Health Technology R&D Project through the Korea Health Industry Development Institute (KHIDI), funded by the Ministry of Health & Welfare, Republic of Korea (Grant number: HI14C1324, HN21C0163, HI21C1576, and HN21C0281), KRIBB Research Initiative Program, the Basic Science Research Program through the National Research Foundation of Korea funded by the Ministry of Education (NRF-2016R1A6A3A11934092 and NRF-2016R1A6A3A11932977), the Graduate School of YONSEI University Research Scholarship Grants in 2017.

Appendix A. Supplementary material

Supplementary data to this article can be found online at https://doi.org/10.1016/j.bioorg.2022.105664. These data include MOL files and InChiKeys of the most important compounds described in this article.

References

[1] S. Frame, P. Cohen, GSK3 takes centre stage more than 20 years after its discovery, Biochem. J. 359 (Pt 1) (2001) 1–16.
[2] B.W. Doble, J.R. Woodgett, GSK-3: tricks of the trade for a multi-tasking kinase, J. Cell Sci. 116 (Pt 7) (2003) 1175–1186.
[3] A. Wada, GSK-3 inhibitors and insulin receptor signaling in health, disease, and therapeutics, Front. Biosci. (Landmark Ed) 14 (2009) 1558, https://doi.org/10.2741/3324.
[4] J.A. McCubrey, L.S. Steelman, F.E. Bertrand, N.M. Davis, S.L. Abrams, G. Montalto, A.B. D'Assoro, M. Libra, F. Nicoletti, R. Maestro, J. Basecke, L. Cocco, M. Cervello, A.M. Martelli, Multifaceted roles of GSK-3 and Wnt/beta-catenin in hematopoiesis and leukemogenesis: opportunities for therapeutic intervention, Leukemia 28 (1) (2014) 15–33.
[5] C. Yost, M. Torres, J.R. Miller, E. Huang, D. Kimelman, R.T. Moon, The axis-inducing activity, stability, and subcellular distribution of beta-catenin is regulated in Xenopus embryos by glycogen synthase kinase 3, Genes Dev. 10 (12) (1996) 1443–1454.
[6] M. Peifer, D. Sweeton, M. Casey, E. Wieschaus, wingless signal and Zeste-white 3 kinase trigger opposing changes in the intracellular distribution of Armadillo, Development 120 (2) (1994) 369–380.
[7] K.K. Jernigan, C.S. Cselenyi, C.A. Thorne, A.J. Hanson, E. Tahinci, N. Hajicek, W. M. Oldham, L.A. Lee, H.E. Hamm, J.R. Hepler, T. Kozasa, M.E. Linder, E. Lee, Gbetagamma activates GSK3 to promote LRP6-mediated beta-catenin transcriptional activity, Sci. Signal 3 (121) (2010) ra37.
[8] J. Behrens, J.P. von Kries, M. Kuhl, L. Bruhn, D. Wedlich, R. Grosschedl, W. Birchmeier, Functional interaction of beta-catenin with the transcription factor LEF-1, Nature 382 (6592) (1996) 638–642.
[9] T. Nakamura, F. Hamada, T. Ishidate, K. Anai, K. Kawahara, K. Toyoshima, T. Akiyama, Axin, an inhibitor of the Wnt signalling pathway, interacts with beta-catenin, GSK-3beta and APC and reduces the beta-catenin level, Genes Cells 3 (6) (1998) 395–403.
[10] H.Y. Kim, Y. Yoon, J.H. Yun, K.W. Cho, S.H. Lee, Y.M. Rhee, H.S. Jung, H.J. Lim, H. Lee, J. Choi, J.N. Heo, W. Lee, K.T. No, D. Min, K.Y. Choi, CXXC5 is a negative-feedback regulator of the Wnt/beta-catenin pathway involved in osteoblast differentiation, Cell Death Differ. 22 (6) (2015) 912–920.
[11] T. Andersson, E. Södersten, J.K. Duckworth, A. Cascante, N. Fritz, P. Sacchetti, I. Cervenka, V. Bryja, O. Hermanson, CXXC5 Is a Novel BMP4-regulated Modulator of Wnt Signaling in Neural Stem Cells, J. Biol. Chem. 284 (6) (2009) 3672–3681.
[12] H.Y. Kim, S. Choi, J.H. Yoon, H.J. Lim, H. Lee, J. Choi, E.J. Ro, J.N. Heo, W. Lee, K. T. No, K.Y. Choi, Small molecule inhibitors of the Dishevelled-CXXC5 interaction are new drug candidates for bone anabolic osteoporosis therapy, EMBO Mol. Med. 8 (4) (2016) 375–387.
[13] S.H. Lee, M.Y. Kim, H.Y. Kim, Y.M. Lee, H. Kim, K.A. Nam, M.R. Roh, D.S. Min, K. Y. Chung, K.Y. Choi, The Dishevelled-binding protein CXXC5 negatively regulates cutaneous wound healing, J. Exp. Med. 212 (7) (2015) 1061–1080.
[14] S.H. Lee, S.H. Seo, D.H. Lee, L.Q. Pi, W.S. Lee, K.Y. Choi, Targeting of CXXC5 by a Competing Peptide Stimulates Hair Regrowth and Wound-Induced Hair Neogenesis, J, Invest. Dermatol. 137 (11) (2017) 2260–2269.
[15] R.A. Blaheta, H. Nau, M. Michaelis, J. Cinatl Jr., Valproate and valproate-analogues: potent tools to fight against cancer, Curr. Med. Chem. 9 (15) (2002) 1417–1433.
[16] S.-H. Lee, M. Zahoor, J.-K. Hwang, D.S. Min, K.-Y. Choi, L.R. James, Valproic acid induces cutaneous wound healing in vivo and enhances keratinocyte motility, PLoS ONE 7 (11) (2012) e48791.
[17] E. Damiens, B. Baratte, D. Marie, G. Eisenbrand, L. Meijer, Anti-mitotic properties of indirubin-3'-monoxime, a CDK/GSK-3 inhibitor: induction of endoreplication following prophase arrest, Oncogene 20 (29) (2001) 3786–3797.
[18] X.J. Ji, F.R. Zhang, Y. Liu, Q.M. Gu, Studies on the antineoplastic action of N-methylisoindigotin, Yao Xue Xue Bao 20 (4) (1985) 247–251.
[19] X.J. Ji, F.R. Zhang, Studies on antineoplastic action of indirubin derivatives and analogs and their structure-activity relationships, Yao Xue Xue Bao 20 (2) (1985) 137–139.
[20] L. Meijer, A.-L. Skaltsounis, P. Magiatis, P. Polychronopoulos, M. Knockaert, M. Leost, X.P. Ryan, C.A. Vonica, A. Brivanlou, R. Dajani, C. Crovace, C. Tarricone, A. Musacchio, S.M. Roe, L. Pearl, P. Greengard, GSK-3-selective inhibitors derived from Tyrian purple indirubins, Chem. Biol. 10 (12) (2003) 1255–1266.
[21] N. Mahindroo, C. Punchihewa, A.M. Bail, N. Fujii, Indole-2-amide based biochemical antagonist of Dishevelled PDZ domain interaction down-regulates Dishevelled-driven Tcf transcriptional activity, Bioorg. Med. Chem. Lett. 18 (3) (2008) 946–949.
[22] S. Choi, H.-Y. Kim, P.-H. Cha, S.H. Seo, C. Lee, Y. Choi, W. Shin, Y. Heo, G. Han, W. Lee, K.-Y. Choi, CXXC5 mediates growth plate senescence and is a target for enhancement of longitudinal bone growth, Life Sci. Alliance 2 (2) (2019) e201800254, https://doi.org/10.26508/lsa:201800254.
[23] G.N. Kumar, S. Surapaneni, Role of drug metabolism in drug discovery and development, Med. Res. Rev. 21 (5) (2001) 397–411.
[24] L. Di, E.H. Kerns, X.J. Ma, Y. Huang, G.T. Carter, Applications of high throughput microsomal stability assay in drug discovery, Comb. Chem. High Throughput Screen 11 (6) (2008) 469–476.
[25] J. Lin, J.R. Cashman, N-oxygenation of phenethylamine to the trans-oxime by adult human liver flavin-containing monooxygenase and retroreduction of phenethylamine hydroxylamine by human liver microsomes, J. Pharmacol. Exp. Ther. 282 (3) (1997) 1269–1279.
[26] S. Choi, K.-Y. Choi, Screening-based approaches to identify small molecules that inhibit protein-protein interactions, Expert Opin. Drug Dis. 12 (3) (2017) 293–303.
[27] K.A. Chuang, C.H. Lieu, W.J. Tsai, M.H. Wu, Y.C. Chen, J.F. Liao, C.C. Wang, Y. C. Kuo, Evaluation of anti-Wnt/beta-catenin signaling agents by pGL4-TOP transfected stable cells with a luciferase reporter system, Braz. J. Med. Biol. Res. 43 (10) (2010) 931–941.
[28] K.M. Jacobs, S.R. Bhave, D.J. Ferraro, J.J. Jaboin, D.E. Hallahan, D. Thotala, GSK-3beta: A Bifunctional Role in Cell Death Pathways, Int. J. Cell Biol. 2012 (2012), 930710.
[29] F. Takahashi-Yanaga, T. Sasaguri, Drug development targeting the glycogen synthase kinase-3beta (GSK-3beta)-mediated signal transduction pathway: inhibitors of the Wnt/beta-catenin signaling pathway as novel anticancer drugs, J. Pharmacol. Sci. 109 (2) (2009) 179–183.
[30] H.-J. Lee, N. Wang, D.-L. Shi, J. Zheng, Sulindac inhibits canonical Wnt signaling by blocking the PDZ domain of the protein Dishevelled, Angew. Chem. Int. Ed. Engl. 48 (35) (2009) 6448–6452.
[31] C. Gao, Y.G. Chen, Dishevelled: The hub of Wnt signaling, Cell. Signal. 22 (5) (2010) 717–727.
[32] S. Ma, J. Choi, X. Jin, H.-Y. Kim, J.-H. Yun, W. Lee, K.-Y. Choi, K.T. No, Discovery of a small-molecule inhibitor of Dvl-CXXC5 interaction by computational approaches, J. Comput. Aided Mol. Des. 32 (5) (2018) 643–655.
[33] I. Lee, S. Choi, J.-H. Yun, S.H. Seo, S. Choi, K.-Y. Choi, W. Lee, Crystal structure of the PDZ domain of mouse Dishevelled 1 and its interaction with CXXC5, Biochem. Biophys. Res. Commun. 485 (3) (2017) 584–590.
[34] T.J. Oldfield, R.E. Hubbard, Analysis of C alpha geometry in protein structures, Proteins 18 (4) (1994) 324–337.
[35] D.L. Zhang, L.J. Gu, L. Liu, C.Y. Wang, B.S. Sun, Z. Li, C.K. Sung, Effect of Wnt signaling pathway on wound healing, Biochem. Biophys. Res. Commun. 378 (2) (2009) 149–151.
[36] C. Bergmann, A. Akhmetshina, C. Dees, K. Palumbo, P. Zerr, C. Beyer, J. Zwerina, O. Distler, G. Schett, J.H. Distler, Inhibition of glycogen synthase kinase 3beta induces dermal fibrosis by activation of the canonical Wnt pathway, Ann. Rheum. Dis. 70 (12) (2011) 2191–2198.
[37] V.M. Schoop, N.E. Fusenig, N. Mirancea, Epidermal organization and differentiation of HaCaT keratinocytes in organotypic coculture with human dermal fibroblasts, J, Invest. Dermatol. 112 (3) (1999) 343–353.
[38] Y. Tanaka, H. Uchi, T. Ito, M. Furue, Indirubin-pregnane X receptor-JNK axis accelerates skin wound healing, Sci. Rep. 9 (1) (2019) 18174.
[39] A.D. Sklirou, N. Gaboriaud-Kolar, I. Papassideri, A.L. Skaltsounis, I.P. Trougakos, 6-bromo-indirubin-3'-oxime (6BIO), a Glycogen synthase kinase-3beta inhibitor, activates cytoprotective cellular modules and suppresses cellular senescence-mediated biomolecular damage in human fibroblasts, Sci. Rep. 7 (1) (2017) 11713.
[40] S. Leclerc, M. Garnier, R. Hoessel, D. Marko, J.A. Bibb, G.L. Snyder, P. Greengard, J. Biernat, Y.Z. Wu, E.M. Mandelkow, G. Eisenbrand, L. Meijer, Indirubins inhibit glycogen synthase kinase-3 beta and CDK5/p25, two protein kinases involved in abnormal tau phosphorylation in Alzheimer's disease. A property common to most cyclin-dependent kinase inhibitors? J. Biol. Chem. 276 (1) (2001) 251–260.